

# Structure determinations for random-tiling quasicrystals

C. L. Henley\*, V. Elser, and M. Mihalkovič\*

LASSP, Cornell University, Ithaca NY 14853-2501.

Received ; accepted

**Abstract.** How, in principle, could one solve the atomic structure of a quasicrystal, modeled as a random tiling decorated by atoms, and what techniques are available to do it? One path is to solve the phase problem first, obtaining the density in a higher dimensional space which yields the *averaged* scattering density in 3-dimensional space by the usual construction of an incommensurate cut. A novel direct method for this is summarized and applied to an *i*(AlPdMn) data set. This averaged density falls short of a true structure determination (which would reveal the typical *unaveraged* atomic patterns.) We discuss the problematic validity of inferring an ideal structure by simply factoring out a “perp-space” Debye-Waller factor, and we test this using simulations of rhombohedral tilings. A second, “unified” path is to relate the measured and modeled intensities directly, by adjusting parameters in a simulation to optimize the fit. This approach is well suited for unifying structural information from diffraction and from minimizing total energies derived ultimately from ab-initio calculations. Finally, we discuss the special pitfalls of fitting random-tiling decagonal phases.

## 1 Introduction

The “random tiling” model of quasicrystals has specific and sometimes radical implications for the procedures that should be used to determine the atomic structures. This paper collects several kinds of answer to the question, “How should one modify the standard crystallographic procedures in order to solve the atomic structure of a random tiling quasicrystal?” (Notice that even the definition of “solve” is arguable in the case of an intrinsically random structure.) We intend this paper to encourage crystallographers to try random-tiling fits to diffraction data, by showing that a couple of approaches have already been thought out in some detail. It also cautions against some common misunderstandings about this point, and collects three new (and imperfectly digested) numerical tests of our ideas. The discussion goes well beyond its antecedent in Sec. 7 of Ref. [1].

### 1.1 Perp space and diffraction

The “perp” coordinate  $\mathbf{h}^\perp$  is a central notion in quasicrystallography. Before proceeding, we had better remind the reader that it has two definitions, which coincide for the case of an ideal tiling.

*Definition 1*, valid for the usual higher-dimensional “cut” description [2] of any quasiperiodic structure (e.g. an ideal tiling). The (periodic) higher-dimensional density consists of atomic surfaces extending in the perp direction; then  $\mathbf{h}^\perp$  is the perp-space displacement from the intersection of the cut plane and the atomic surface, to a vertex of the higher-dimensional lattice.

*Definition 2*, valid for any arbitrary (e.g. random) tiling. Any tiling can be “lifted” so that each tile vertex maps to a vertex of a periodic lattice in a higher dimension [1, 3]; then  $\mathbf{h}^\perp$  of each tile vertex is the difference between the perp component of its lattice vector and the mean value (“center-of-mass” in perp space).

Consider the probability distribution of the Definition 2  $\mathbf{h}^\perp$  values. It is easy to check that, as long as the physical (hyper)plane has an irrational orientation, and in the limit of a large physical-space volume  $V$ , there are  $n_0 V d^3 \mathbf{h}^\perp$  possible perp-space points in a perp volume element  $d^3 \mathbf{h}^\perp$ , where  $n_0^{-1}$  is the volume of the unit cell in the  $d$ -dimensional lattice. The mean number of such points actually present in the tiling is defined to be  $\rho(\mathbf{h}^\perp) n_0 V d^3 \mathbf{h}^\perp$ , so  $\rho(\mathbf{h}^\perp) \in [0, 1]$  is a probability. In random tilings it is, in practice, a smooth function. (In the special case of an ideal tiling,  $\rho(\mathbf{h}^\perp)$  is 1 within the “acceptance domain” where sites are sure to be occupied, and zero outside it.) Note  $\mathbf{h}^\perp$ , according to Definition 1, or its mean  $\bar{\mathbf{h}}^\perp \equiv \int d^3 \mathbf{h}^\perp \mathbf{h}^\perp \rho(\mathbf{h}^\perp)$  according to Definition 2, plays the role for perp displacements that a crystal’s center-of-mass plays for ordinary displacements.

Now, we may take an ensemble average of a random tiling ensemble, just constraining the value  $\bar{\mathbf{h}}^\perp$  to be zero (without loss of generality). This gives, in real space, a nonzero density  $\rho(\mathbf{r})$  on a discrete (but dense) set of points  $\mathbf{r}$ . It is a fact, natural though not rigorously proven, that  $\rho(\mathbf{r})$  depends only on the perp-coordinate  $\mathbf{h}^\perp$  of the point  $\mathbf{r}$ . If so, it is easy to see  $\rho(\mathbf{r}) = \rho(\mathbf{h}^\perp)$  as defined in the last paragraph. In other words, starting with Definition 2, we found the averaged density  $\rho(\mathbf{r})$  is given by the cut construction of Definition 1, if the atomic surfaces are weighted by  $\rho(\mathbf{h}^\perp)$ .

\* Correspondence author (e-mail: clh@ccmr.cornell.edu) Please also note that M.M.’s present address is Materials Research and Liquids, Institute of Physics, TU Chemnitz, D-09107 Chemnitz, Germany; his permanent address, Institute of Physics, Slovak Academy of Sciences, 84228 Bratislava, Slovakia.

This shows that  $\rho(\mathbf{r})$  is quasiperiodic, since that term is, practically speaking, *defined* by the existence of a cut construction.<sup>1</sup>

These facts about  $\rho(\mathbf{h}^\perp)$  easily generalize to atomic decorations in which atoms sit on some of the tile vertices. Thus wherever the physical 3-plane cuts an atomic surface,  $\rho(\mathbf{h}^\perp)$  is the probability that an atom is present.

The Bragg component of the diffraction amplitude  $F_{\mathbf{g}}$  is defined as the part which scales as  $V$  with the volume. It is, in fact, simply the Fourier transform of the averaged density: [3],

$$F(\mathbf{g}^\perp) = \int d^3\mathbf{h}^\perp \rho(\mathbf{h}^\perp) e^{-i\mathbf{g}^\perp \cdot \mathbf{h}^\perp} \quad (1)$$

Here  $\mathbf{g}^\perp$  is the perp-space partner of the reciprocal lattice wavevector  $\mathbf{g}$ . In cases other than icosahedral, “3” in eq. (1) is replaced by “ $d_\perp$ ”, the dimensionality of perp space. (However we shall assume the physical dimension is always 3, since this paper considers determinations from Bragg peaks, but random tilings have no Bragg peaks in dimension 1 or 2.) For a tiling decorated by real atoms, (1) can be suitably generalized by including form factors and allowing for different classes of site (see eq. (27), below).

## 1.2 Random tilings and the cut description

Bragg diffraction amplitudes are always represented by a quasiperiodic density in higher-dimensional space, which when cut by a 3-plane at the correct incommensurate orientation gives the diffracting density in physical space. [2] The crystallographic refinements done to date have presupposed that the structure, ideally, *is* quasiperiodic. But an (at least) equally plausible scenario is that the thermal equilibrium structure is an intrinsically random tiling and so that its long-range quasiperiodic order is stabilized by the tiling’s configurational entropy. [5, 1] Notions concerning the free energy and elastic constants are central to the *physics* [5, 1] but will not be repeated here since they are somewhat tangential to the *crystallography*. Indeed, large parts of this paper could be applied equally well to the cases of (i) the “icosahedral glass” [6], e.g.  $i(\text{AlCuLi})$ , or  $i(\text{TiNiZr})$ , which is not thermodynamically stable; or (ii) the “weak matching-rule” quasicrystal [7], which is a slight generalization of the ideal, energetically stabilized quasicrystal that nevertheless has a nonzero density of intrinsically random sites.

So, how does the cut description get modified in the case of a random tiling? As just noted in Sec. 1.1, the physical-space density giving rise to the Bragg amplitudes is the ensemble average of the scattering density. This average is perfectly quasiperiodic, and so even for a random tiling it is represented as a cut by a 3-plane through a function in a higher-dimensional space.

However, the physical-space density will have a great many fractionally occupied atoms; even if there is no substitutional disorder, since a given volume of space has probabilities to be divided into tiles in different ways and different tiles have different decorations. A second effect is

the “physical-space displacements” [8], the deviations of an atom from ideal tiling vertex positions in response to forces from neighboring atoms. In ideal structures, an atom’s local environment is a deterministic function of  $\mathbf{h}^\perp$ . Then the atom’s equilibrium position is  $\mathbf{r}_0 + \mathbf{u}(\mathbf{h}^\perp)$ , also a function of  $\mathbf{h}^\perp$ , and this is the parametrization of the atomic surface’s shape. In the random case, however, atoms corresponding to the same  $\mathbf{h}^\perp$  can have different local environments and hence different parallel-space displacements. This manifests itself as split positions in the physical-space cut, or equivalently the atomic surface becomes an discrete family of surfaces, displaced from each other by small offsets in parallel space, and each having its own distribution  $\rho(\mathbf{h}^\perp)$ .

Crystallographers would sometimes argue that a Fourier map reconstructing the correct ensemble-average density *is* “the structure” and is the proper goal when we fit the diffraction. In other words, they would say the task is done as soon as the phase problem is solved. We disagree strongly with this viewpoint. The aim of structural studies is to uncover the actual structure, which means understanding what a typical realization is like and not just the average over realizations. If the averaged structure contains two nearby, half-occupied sites, does the actual structure contain exactly one atom which can occupy either site at random? Or is it that 50% of the time *both* sites are occupied, and at other times some other site is occupied? Spurious but rare sites have negligible effect on the  $R$ -factor, but major effects on the total energy and the electronic states computed from the structure. Hence, the goal should be a proper description of the entire ensemble of configurations.

## 1.3 Outline of the paper

There are two alternate approaches for solving a random tiling structure:

1. “*Standard*” approach. Break up the task into two stages. The first stage is to solve the phase problem without a complete model of the real-space structure. The (averaged) scattering density  $\rho(\mathbf{r})$  can then be constructed as an incommensurate cut in a high-dimensional space. The second stage is to relate this density to an atomic model.

2. “*Unified*” approach. Assume a particular kind of random-tiling model, with variable parameters (such as the positions and species of decorating atoms on the tiles, or coefficients in the “tile Hamiltonian” that governs the statistics of patterns in the random tiling). Simulate the tiling, calculate the Bragg intensities, and calculate an  $R$  factor to measure its deviation from the measured intensities. Adjust the parameters in a direction that will reduce  $R$  and repeat the simulation; iterate until a good fit is achieved. Following this path, the phase solution is unified with the structure fitting; it is also natural to unify the  $R$ -factor from diffraction and the total energy in a combined objective function to be minimized by the fit.

Most of this paper is devoted to elaborating the two approaches. We begin with the “standard” path in sec. 2, focusing on the new “minimum-charge” method, a direct method for determining the phases of a general structure. This method is not peculiar to quasicrystals, nor to random structures. However, the minimum-charge viewpoint is useful for random structures since it provides an inequality for

<sup>1</sup> In the case of the two-dimensional equilibrium random tiling or the icosahedral glass, the above arguments break down because  $\rho(\mathbf{h}^\perp) = 0$ , i.e. the distribution gets broader and broader with increasing  $V$ .

the diffuse scattering (Sec. 2.2) which allows us to quantify the degree of disorder without solving the structure, even partially. Also, preliminary calculations using the minimum-charge approach have suggested the structure of  $i(\text{AlPdMn})$  is more disordered than any of us had believed.

As we have just argued, even a perfect solution of the phase problem is very far from giving a useful model of the structure. This gap can be bridged by the brutally simple “factorization approximation”: assuming that the intensities are those of ideal structure apart from a (Gaussian) “perp Debye-Waller” factor. This is critiqued and tested by simulations in Sec. 3.

After Sec. 3 we turn to the “unified” path. We first review key notions of tile-decorations (Sec. 4), since these are used to specify random-tiling structures, practically by the definition of a random tiling. Then Sec. 5 describes several fitting procedures, beginning with a recipe for discovering the appropriate random tiling model by simulations (provided a set of interatomic pair potentials is known). Finally, we explain in Sec. 6 the special problems posed by decagonal structures.

Our subject is *not* the long-wavelength “phason” elasticity which produces diffuse wings around the Bragg peaks. These phenomena indeed characterize “random tiling” type behavior, but as argued previously in Ref. [1], one should *not* necessarily think this accounts for most of the disorder. A priori, one expects that the disorder is mostly correlated at the scale of a tile edge or so; these correlations are controlled by the constraints of the tiling rules, and produce diffuse scattering which is not associated with particular Bragg peaks.

## 2 Solving the phase problem

The “standard” approach to structure solution begins by first solving the phase problem. This step is somewhat different than for ordinary crystals, but it seems not to matter much whether the quasicrystal is modeled as ideal or as a random tiling.

We first mention a couple of well-known techniques. An old technique [9] takes advantage of the smooth dependence of the structure factor  $F_{\mathbf{g}}$  when plotted as  $F(\mathbf{g}^{\perp})$ , where  $\mathbf{g}^{\perp}$  is the perp-space partner of  $\mathbf{g}$ . Where  $|F(\mathbf{g}^{\perp})|$  passes through a zero, one infers that  $F(\mathbf{g}^{\perp})$  must change sign. Another approach, described by Qiu and Jarić, was to discover phases using known rational approximant crystals (by expressing them as rational cuts of a higher-dimensional structure). [10].

In the rest of this section, we first outline a new approach, the “minimum-charge” method (Sec. 2.1). Quite independent of this, we derive an inequality which is useful as a diagnostic of disorder (Sec. 2.2). Finally, we apply both of these ideas to a data set for  $i(\text{AlPdMn})$ , in Sec. 2.3.

### 2.1 “Minimum-charge” approach

A promising new “direct method” (not specific to quasicrystals) to solve the X-ray diffraction phase problem was suggested by one of us [11]. The key notion of this is to min-

imize the average electron charge density. Any periodic or quasiperiodic density has the form

$$\rho(\mathbf{r}) = F_0 + \sum_{\mathbf{g} \neq 0} |F_{\mathbf{g}}| \cos(\mathbf{g} \cdot \mathbf{r} - \phi_{\mathbf{g}}), \quad (2)$$

where  $F_0$  is the average density;  $|F_{\mathbf{g}}| \propto \sqrt{I_{\mathbf{g}}}$  and  $\phi_{\mathbf{g}}$  are the magnitudes and phases of structure factors. The former are obtainable from the measured intensities  $I_{\mathbf{g}}$  and the latter are to be determined. The “minimum charge” method [11] considers the reduced density

$$\tilde{\rho}(\mathbf{r}) \equiv \rho(\mathbf{r}) - F_0, \quad (3)$$

and seeks phases  $\phi_{\mathbf{g}}$  which maximize the minimum value of  $\tilde{\rho}(\mathbf{r})$

$$\tilde{\rho}_{\min} = \min_{\mathbf{r}} \tilde{\rho}(\mathbf{r}). \quad (4)$$

The minimum value of  $F_0$  which makes  $\rho(\mathbf{r})$  everywhere nonnegative is then  $F_0 = -\tilde{\rho}_{\min}$ . It is straightforward to argue that at an optimal set of  $N$  phases (where  $F_0$  has achieved a local minimum) the minimum  $\tilde{\rho}_{\min}$  is attained at  $N + 1$  exactly degenerate local minima of  $\tilde{\rho}(\mathbf{r})$ . Consequently, for optimal phases, the minimum “background” value of the density is found in large regions of the unit cell. If some phase assignment allows for the volume occupied by this background density to be especially large, as we expect when dealing with a true atomic density, the corresponding value of  $F_0$  will be especially low. This property distinguishes the global minimum of  $F_0$  and provides for an unambiguous phase solution.

By sampling  $\tilde{\rho}(\mathbf{r})$  on a “Fourier grid” [12] of a comparable size, the charge minimization problem, say for a centrosymmetric space group, is cast into a mixed integer programming optimization [13] for the unknown (integer) signs and (real valued)  $F_0$ . Because of linearity (of objective function and constraints) there are efficient search strategies for this general class of problem. For the  $i(\text{AlPdMn})$  x-ray phases (see Subsec. 2.3) the “branch and bound” technique was used, where the relaxation of the constraint  $|s_{\mathbf{g}}| = 1$  (on each of the signs) to the weaker statement  $|s_{\mathbf{g}}| \leq 1$  (on a subset of the signs) provides bounds on the objective function ( $F_0$ ) that frequently are strong enough to eliminate large branches of the search tree.

There is a similarity between the minimum charge (*minQ*) and the maximum entropy (*maxS*) methods. Both succeed in eliminating or minimizing wiggles in the electron density in regions where there should be no charge. The similarity is only superficial, however. On the one hand, *maxS* is fundamentally a strategy for refining phases which are already approximately determined, but corrupted by noise; on the other hand, *minQ* makes perfect sense in the context of perfect data. Also, *minQ* was developed specifically for *ab initio* phase determination, whereas the application of *maxS* in this mode has no theoretical basis.

### 2.2 Inequalities for X-ray structure factors

The aim of this subsection is to place a lower bound on the amount of disorder, taking advantage of the fact that the

density of scattering electrons is nonnegative. This is completely independent of the preceding section and, in particular, all the conclusions of Subsec. 2.2 can be drawn without ever determining or even considering a single phase factor.

The positivity of  $\rho(\mathbf{r})$  implies the inequality

$$|F_{\mathbf{g}}| = |\langle \rho(\mathbf{r}) e^{-i\mathbf{g}\cdot\mathbf{r}} \rangle_r| \leq \langle |\rho(\mathbf{r})| \rangle_r = F_0, \quad (5)$$

where  $\langle \dots \rangle_r$  means a *spatial* average. It should be emphasized that  $\rho(\mathbf{r})$  already contains an *ensemble* average: that is just what the Bragg scattering represents, as we noted in Sec. 1.1. Eq. (5) is the most trivial of the Harker-Kasper inequalities [14]. Note, though, that in crystallography, these (and later inequalities) were always applied to the solution of the phase problem assuming an ideal structure. We apply (5) instead as a rigorous diagnostic of a *disordered* structure, using only Bragg (not diffuse) scattering.

It follows very obviously from (5) that  $|F_{\mathbf{g}}|/\sqrt{\sum |F_{\mathbf{g}}|^2} \leq |F_0|/\sqrt{\sum |F_{\mathbf{g}}|^2}$  which is conveniently written

$$\frac{|F_{\mathbf{g}}|}{\sqrt{\sum_{\mathbf{g} \neq 0} |F_{\mathbf{g}}|^2}} \leq \alpha \quad (6)$$

where

$$\alpha \equiv \frac{F_0}{\sqrt{\sum_{\mathbf{g} \neq 0} |F_{\mathbf{g}}|^2}}. \quad (7)$$

Note that  $\alpha$  just depends on the first two moments of  $\rho$ , since

$$\langle \rho \rangle_r = F_0, \quad (8)$$

$$\langle \rho^2 \rangle_r = F_0^2 + \sum_{\mathbf{g} \neq 0} |F_{\mathbf{g}}|^2. \quad (9)$$

The value of (6) is that both sides can be related to experimentally measurable data, as is evident for the Bragg intensities in the left hand side. (The sum omits  $F_0$ , which is not measurable as a Bragg intensity.) The right hand side turns out to depend only on atomic parameters such as charges, number density, concentrations, etc., which are known from the composition, *provided we assume the diffracting material consists of a known density of definite atomic species* (well separated so overlaps of atomic charge distributions are negligible). Specifically, suppose there is no disorder other than that due to thermal vibrations of the atoms. To a good approximation one may then represent the electron density as a sum of non-overlapping distributions centered around each atom,  $\rho^{\text{atom}}_i(\mathbf{r})$  where  $i$  is the atomic species. Without knowing the atomic positions, it is possible to evaluate the averages in (8) and (9):

$$\langle \rho \rangle_r = n \sum_i x_i Q_i \quad (10)$$

$$\langle \rho^2 \rangle_r = n \sum_i x_i P_i, \quad (11)$$

where  $n$  is the number density of atoms,  $x_i$  the atomic composition, and

$$Q_i = \int \rho^{\text{atom}}_i(\mathbf{r}) d^3\mathbf{r} \quad (12)$$

$$P_i = \int \rho^{\text{atom}}_i(\mathbf{r})^2 d^3\mathbf{r}. \quad (13)$$

Inserting (10) and (11) into the earlier equations, (8) and (9), we conclude  $\alpha = \alpha_0$ , where

$$\alpha_0 \equiv \frac{1}{\sqrt{\frac{\sum x_i P_i}{n(\sum x_i Q_i)^2} - 1}}. \quad (14)$$

is expressed purely in terms of the atomic parameters  $n$ ,  $x_i$ ,  $Q_i$  and  $P_i$ .

Our inequality (6) is rigorous. If it is violated by the value of  $\alpha_0$  computed from the data, it means we were mistaken in our assumption that the electron density  $\rho(\mathbf{r})$  has 100% occupation of every site and no chemical disorder. Let us repeat the derivation above, assuming a distribution of occupations (in the case of a single species for simplicity). In place of (14) we find

$$\alpha \simeq \sqrt{\frac{nQ^2}{P\langle y \rangle_z}}, \quad (15)$$

in the case where  $\alpha \ll 1$ . Here  $z(y)$  is the distribution of the fraction of charge from sites with fractional occupation  $y$ . Disorder decreases  $\langle y \rangle$  and thereby, according to (15), increases  $\alpha$  beyond the value in (14). If we allow for enough occupational disorder, inequality (6) will be satisfied.

### 2.3 Example: the $i(\text{AlPdMn})$ density map

Recently[15] the “minimum-charge” method was applied to determine the phases for  $i(\text{AlPdMn})$ , which has the centrosymmetric space group  $F\bar{5}3\frac{2}{m}$ , from the x-ray data of Boudard et al.[16]. This data set has 503 symmetry inequivalent reflections, 360 having  $\sigma_{\mathbf{g}}/I_{\mathbf{g}} < 0.5$ ; we used all the reflections.

Figures 1 and 2 both show the reconstructed electron density using signs obtained with the minimum charge method. Slices through physical space (Fig. 1), and along rational planes (Fig. 2), both show disorder, as we argue in the next two paragraphs. Disorder of this sort is expected in a random tiling, but our observations here do not rule out other origins.

Figure 1(a) shows the electron density in a 2-fold (mirror) plane of physical space, centered on the “ $n_0$ ” atomic surface. While a subset of the atoms corresponds exactly to the Mackay cluster second shell (12+30 atoms), we see that there are also several pairs of well defined atoms having unphysically short separations. Similar evidence of split positions has been noted before by others, but was never ruled definitive because of the possibility of being a truncation artifact[17]. Because of the flatness of the background in these reconstructed densities we feel that truncation cannot be invoked to explain these examples of split positions. A preliminary survey of the reconstructed density suggests that split positions are actually quite common.

In the periodic 5-fold plane (Fig. 2) we see three atomic surfaces centered at Wyckoff positions with icosahedral symmetry. The positions and net charge in these surfaces are consistent with the “spherical model” of Boudard et al[16]. We observe, however, that the density profiles of all three surfaces are very rounded, rather than step-

function-like.<sup>2</sup> The width of the appropriate broadening function in the factorization approximation (see eq. (19), below) would be comparable in magnitude to the diameter of the largest (ideal) atomic surface in the spherical model. This explains, for example, why the sizes of the largest (“ $n_0$ ”) and smallest (“ $bc_1$ ”) surfaces of Ref. [16] are comparable in our image, whereas in the spherical model their diameters are in the ratio 2.3:1.

Even before determining the phases, the Boudard data[16] can be manipulated to show (using the inequalities in Sec. 2.2) that the  $i(\text{AlPdMn})$  phase possesses considerable partial/mixed occupational disorder. To evaluate  $\alpha$  from eq. (14), we first approximated the atomic form factor for each species  $i$  as a Gaussian,

$$\rho^{\text{atom}}_i(\mathbf{q}) = Q_i e^{-\frac{1}{2}B_i|\mathbf{q}|^2}, \quad (16)$$

with the parameters  $B_i$  chosen to reproduce the integrals  $P_i$  in (13) obtained using Hartree-Fock wavefunctions. This gave  $B_{\text{Al}} = 0.012$ ,  $B_{\text{Pd}} = 0.0042$ , and  $B_{\text{Mn}} = 0.007$  (in units of  $\text{\AA}^2$ ). Since  $B_{\text{Pd}}$  is close to the measured Debye-Waller factor for Pd[18],  $B_{\text{DW}} = 0.0044$ , the thermally averaged distribution for Pd is better represented by a Gaussian with  $B = 0.0086$ . Since Pd atoms make the main contribution to  $\alpha$ , we used the same Debye-Waller factor to correct the Al and Mn distributions. Using the measured composition and density[16], we finally arrive at  $\alpha_0 = 0.0439$ .

The sum  $\sum |F_{\mathbf{g}}|^2$  in (6) is in principle determined by a measurement of all the Bragg intensities. Barring surprises in the unexplored regions of reciprocal space, we believe the intensities that have been measured exhaust this sum: the weaker measured peaks of our data set already make a negligible contribution to it, and peaks with larger  $\mathbf{g}$  or  $\mathbf{g}^\perp$  are cut off by Debye-Waller factors. Our conclusion about the disorder follows from the fact If we assumed no disorder, then  $\alpha = \alpha_0$  and the three most intense reflections (18/29, 52/84, and 20/32) would violate inequality (6) by as much as 40%. Our estimate of disorder is certainly conservative since there is no reason to expect that inequality (5) would be close to an equality. (Sec. 3.1.1 also indicates a large disorder in this material.)

### 3 Factorization approximation

The determination of the phases, and hence of the averaged scattering density, is not the end of the structure determination in the random-tiling case. A process of simulation and fitting is still called for. (See Sec. 5, below.) The factorization approximation – equivalently the “Phason Debye-Waller factor” – is a shortcut of dubious validity, which is nevertheless attractive since it offers the hope of relating the data to an ideal model with much less effort.

In fitting diffraction, it was natural to generalize the Debye-Waller factor to perp space and to assume

$$F_{\mathbf{g}}^{\text{rand}} = F_{\mathbf{g}}^{\text{ideal}} e^{-W(\mathbf{g})} \quad (17)$$

for the Fourier amplitudes of the random and ideal tilings (labeled by “rand” and “ideal” henceforth). Here the “perp Debye-Waller factor” is given by

$$W(\mathbf{g}) = \sigma^2 |\mathbf{g}^\perp|^2 / 2 \quad (18)$$

where  $\mathbf{g}^\perp$  is the perp-space wavevector corresponding to  $\mathbf{g}$ . We will call this the “factorization approximation”. In direct (perp) space, in view of (1), eq. (17) is equivalent, for an icosahedral quasicrystal, to

$$\rho^{\text{rand}}(\mathbf{h}^\perp) = \int d^3 \mathbf{u}^\perp w(\mathbf{u}^\perp) \rho^{\text{ideal}}(\mathbf{h}^\perp - \mathbf{u}^\perp) \quad (19)$$

where  $w(\mathbf{u}^\perp)$  is a (normalized) smearing function with a Gaussian profile:

$$w(\mathbf{u}^\perp) = (2\pi\sigma^2)^{-3/2} \exp[-|\mathbf{u}^\perp|^2 / 2\sigma^2] \quad (20)$$

Notice that it follows from (19) that the random tiling vertices have a perp variance increased over the ideal tiling by

$$\langle |\mathbf{h}^\perp|^2 \rangle_{\text{rand}} - \langle |\mathbf{h}^\perp|^2 \rangle_{\text{ideal}} = 3\sigma^2. \quad (21)$$

For a general quasicrystal, “3” must be replaced by “ $d_\perp$ ” in eqs. (19) – (21). (We wrote them assuming perp space is three-dimensional as in the icosahedral case.)

It must be borne in mind, however, that there is *no* exact basis for the factorization approximation. One may be misled because elastic theory tells us all *long wavelength* perp fluctuations are Gaussian.<sup>3</sup> But this relation is not useful, since we expect much of the random-tiling disorder to be short-range.

Another way one may be misled is that, when the higher-dimensional cut construction is overemphasized, a natural cartoon of the random tiling is to take the *same* higher-dimensional crystal as in the ideal case, but to permit the cut-surface to undulate – to deviate from being a flat plane. If the cut-surface has Gaussian fluctuations that are completely uncorrelated with the atomic surfaces, then the factorization approximation would become exact. This “undulating cut” notion was critiqued in Sec. 4 of Ref. [1].<sup>4</sup>

The factorization assumption is fundamentally ill-defined since the same random tiling (e.g., of Penrose rhombi) may be obtained as the randomization of *various* different quasiperiodic tilings (e.g. the generalized Penrose tilings in two dimensions) – yet eq. (17) demands that we identify a *particular* ideal tiling as the one which has been

<sup>2</sup> We caution that some important details are lost when the weak reflections are omitted; in other words, truncation error may introduce a spurious apparent randomness. For example, with only 300 reflections the profile of the atomic surface at the center of Fig. 2(b) looks quite Gaussian. (Its correct appearance is two-peaked because its center in perp space is occupied by Mn, while the rest of the atomic surface is Pd which possesses twice as many electrons as Mn.)

<sup>3</sup> This does imply a formula like (19) relating  $\rho^{\text{rand}}(\mathbf{h}^\perp)$  to the coarse-grained distribution  $\rho^{\text{short}}(\mathbf{h}^\perp)$ , obtained after averaging the “center-of-mass” in perp space locally, from a region several tiles wide, rather than over the entire system.

<sup>4</sup> In places where a straight cut would always cross exactly one out of two atomic surfaces, an undulating cut may cross both or neither of them, which produces an overlap or gap between parts of tiles. Additionally, two slightly different undulating cuts often produce the same real structure, so one must be careful in assigning a statistical weighting to the ensemble of undulating cut surfaces.

randomized. The physical meaning of (19) is dubious, too: it says that, when the tiling is randomized, the vertices with a prescribed local environment, which in the ideal tiling have a specific  $\mathbf{h}^\perp$  value, now get shifted by a random offset  $\mathbf{u}^\perp$  which has a probability distribution (20). But there is no reason the random variable  $\mathbf{u}^\perp$  should have the same variance (21), independent of what kind of local environment is in question or of how large is its  $\mathbf{h}^\perp$  location.

We claim the factorization approximation works trivially for sufficiently small  $\mathbf{g}^\perp$ . After all, an integral of form (1) can always be written as  $\exp(-C_0 + \frac{1}{2}C_2|\mathbf{g}^\perp|^2 + \dots)$ , where  $C_{2k}$  is the *cumulant* of order  $2k$  of the density  $\rho(\mathbf{h}^\perp)$ . Then since the  $2k = 4$  term in the exponent is of order  $(\mathbf{g}^\perp)^4$ , it follows that  $F(\mathbf{g}^\perp)$  has a roughly Gaussian shape at small  $\mathbf{g}^\perp$ , even for the ideal tiling (see Ref. [3]). The real test of the factorization approximation is whether it works for larger  $\mathbf{g}^\perp$ , with the fitted  $\sigma^2$  in (18) being independent of  $\mathbf{g}^\perp$ . Surprisingly, this seems to be true for our simulations, as the rest of this section shows.

### 3.1 Simulation tests

We carried out simulations of the completely random tiling of rhombohedra [20, 21, 22], as a toy model to test (for the first time) the relation between diffraction amplitudes in the ideal and random tilings: in particular, to test the validity of Eq. (17). These measurements are preliminary; we hope they can be repeated in the future, more systematically and perhaps on models closer to the real quasicrystals. The rest of this section is devoted to these simulations.

We used the cell of the “8/5” cubic approximant with periodic boundary conditions, which contains 10 336 vertices (an equal number of rhombohedra). For equilibration we allowed 500 Monte Carlo steps (MCS) / vertex (these are flip attempts of which only 17% cause flips), and then our ensemble for diffraction consisted of 1000 sample taken at intervals of 250 MCS/vertex. (This is adequate to decorrelate this maximally random model,<sup>5</sup>

but quite inadequate when there is a Hamiltonian [22].)

A novel detail of our simulation is that periodic boundary conditions are also assumed, rather arbitrarily, in the *perp* direction. Thus, only a finite set of  $(178)^3 \mathbf{h}^\perp$  values is possible. In practice all vertices fall within a smaller domain of these in *perp*-space –  $130^3$  points were used here – and configurations are efficiently represented as a lattice gas on this grid.

#### 3.1.1 Results on *perp*-space distribution

It is possible to visualize the smearing of eq. (19) directly, rather than through the *perp* Debye-Waller factor. On the theory side, it is straightforward to construct a histogram of  $\mathbf{h}^\perp$  values for the vertices of the random rhombohedral tiling (see Sec. 3.1, below). A random-tiling decoration model [38] has been proposed for  $i(\text{AlCuFe})$  and

$i(\text{AlPdMn})$ . This is based on the rhombohedral random tiling, which has simple-icosahedral space group. However, the atomic decoration treats even and odd vertices inequivalently, so the atomic structure is face-centered icosahedral, like the real quasicrystals, and is similar to prior models based on diffraction [9, 16]. In particular, the  $bc_1$  atomic surface is (in this model) made up precisely of atoms that decorate the *even* rhombohedron nodes and should have the same *perp*-space distribution  $\rho(\mathbf{h}^\perp)$  as *all* nodes do in the simulation (since even and odd nodes have the same  $\rho(\mathbf{h}^\perp)$  in this model). In short, the experimental *perp*-space distribution of the  $bc_1$  surface is just a section through the density map (Sec. 2).

Surprisingly, assuming the phase reconstruction is correct,  $i(\text{AlPdMn})$  – the most perfectly ordered quasicrystal to date – appears “more random than random” as quantified by the apparent value of  $\sigma^2$  in Fig. 3. This conclusion is also supported by the quite small numerical values of elastic constants in  $i(\text{AlPdMn})$ , as measured from diffuse scattering [19], in comparison to models [22]. We know only two possible explanations of this disorder, neither of which is very convincing:

*Explanation (i):* The true tiles are deflated compared to the assumed ones by some factor like  $\tau^2$  (such rescalings are discussed in Sec. 9.2.1 of Ref. [1]). But for  $i(\text{AlPdMn})$  this seems impossible, as the true tile edge would be no larger than an interatomic spacing.

*Explanation (ii):* The ratio of elastic constants is close to  $K_2/K_1 = -0.75$  at which a “phason instability” occurs, with a divergence of *perp* fluctuations [26]. Within the entropic-stabilization scenario, such an instability is indeed expected when the temperature is lowered [5] – but only near a critical temperature, not over a wide range.

Further understanding awaits a better understanding of the currently unsettled experimental situation. In particular, Ref. [27] found that the diffuse scattering differed by a factor of 20 between two slightly different samples of  $i(\text{AlPdMn})$ ; it is unclear which of these is like the sample of Ref. [16].

#### 3.1.2 Computing Bragg and diffuse scattering

The rest of our studies in this section depend on the diffraction. To compute this, each vertex was taken to be a point scatterer with form factor unity. In the size 8/5 approximant, computing the Fourier transform at *every* wavevector in the interesting range would take weeks or years of CPU time, so we used lists of selected wavevectors (see below).

When one uses periodic boundary conditions, of course the real reciprocal-space vectors fall on a discrete grid. Due to our special adoption (see above) of *perp* periodic boundary conditions, the *perp* reciprocal-space vectors also lie on a discrete grid. Indeed *each* of our real reciprocal-space vectors  $\mathbf{q}$  is the projection of infinitely many 6D reciprocal-lattice vectors, and can thus be considered as a Bragg vector (with the appropriate distortion since this is an approximant). We select the smallest of these to make the correspondence unique. In practice most of the  $\mathbf{q}$  vectors correspond to such a large  $\mathbf{g}^\perp$  that the Bragg amplitude is zero to computer precision.

<sup>5</sup> The relaxation time of the slowest Fourier mode in the 8/5 cell was found to be only 280 MCS/site [21]. Our Fig. 4 agrees well with Fig. 1 of Ref. [20]; furthermore, a different run with the same protocol yielded elastic constants  $(K_1, K_2) = (0.84, 0.50)$  within 2% of the results for the same size in Ref. [21], Fig. 2.

We defined the “Bragg” and “diffuse” parts of the diffraction according to their behavior in the infinite-size limit, so we need a new operational definition or procedure to separate the Bragg from the diffuse intensity in a fixed, finite lattice. This is easy to do, in view of the discussion in Sec. 1.1: the amplitude’s ensemble average is taken to be the Bragg amplitude, while its variance is the diffuse intensity. However, even if each sample were very similar to the previous one, it is offset by a random fraction of the simulation cell, independent of the previous offset. Hence, before taking the Fourier sum over each sample, we located the “center-of-mass” of its perp-space coordinates, and then uniformly shifted the vertex coordinates (by integer multiples of the underlying grid of the lattice-gas) so as to make this center-of-mass nearly zero.

In this fashion we could measure Bragg intensity even on peaks where the diffuse intensity was perhaps  $\sim 10$  times as big.<sup>6</sup> The results (along a twofold axis) are shown in Fig. 4. Bragg peaks of the ideal tiling are identifiable down to amplitude  $10^{-4}$  relative to the maximum (far smaller than experimentally measurable). Bragg amplitudes of order  $10^{-2}$  in the ideal tiling became of order  $10^{-4}$  in the random tiling, which is about where they become lost in the diffuse noise. In the best experimental data sets, the smallest measured Bragg amplitude is down about  $10^{-2}$  from the largest one.

### 3.2 Results: perp-space Debye-Waller factor

Fig. 5 shows the Bragg intensities plotted against  $|\mathbf{g}^\perp|$  for selected wavevectors; the amplitudes (same data, but with signs) are plotted in the upper panels of Fig. 6. We can define the ratio

$$2W_{\text{eff}} \equiv -\ln [I^{\text{random}}(\mathbf{g})/I^{\text{ideal}}(\mathbf{g})] \quad (22)$$

which is plotted against  $|\mathbf{g}^\perp|^2$  in Fig. 6(a). The straight-line fit confirms (18) with  $\sigma^2 = 0.145$ . On the other hand, the variance  $\langle |\mathbf{h}^\perp|^2 \rangle$  has been (easily) measured for both random and ideal tilings: inserting these numerical values into Eq. (21) gives  $3\sigma^2(1.670) - (1.236) = 3(0.148)$ , in perfect agreement. The only caution to be mentioned is that the deviations which appear small because of the logarithmic scale of Fig. 6, may in fact be far greater than the measurement errors of the intensities. By the time the factorization approximation breaks down completely, at  $|\mathbf{g}^\perp|^2 \approx 25$ , the random-tiling Bragg peaks (see top panel) are too small to measure in a real experiment.

Do the Bragg amplitudes behave differently when there are several orbits with different species of atoms, or when the atoms do not sit on vertices? To check this, we also calculated the diffraction from a decorated model in which atoms with form factor  $+1$  sit on all rhombohedron vertices and another species with  $-1$  sits on mid-edges and also on prolate rhombohedron axes at ideal points corresponding to

body centers of six-dimensional cubes.<sup>7</sup> This places 54 120 atoms in the “8/5” size simulation cell.

The answer – appearing in Figures 5, 6, and 7 – is that the decorated model is the same qualitatively – for example,  $\sigma^2$  is fit to 0.143, essentially the same value. (The fit is just a little bit worse.)

#### 3.2.1 Correctness of the phase?

A special concern was whether the random-tiling amplitude always has the same *sign* as the ideal-tiling. Recall that, as a function of  $|\mathbf{g}^\perp|$ , the ideal-tiling amplitude oscillates and has zero crossings at certain wavevectors. The first zero-crossing of the random-tiling vertices agrees precisely with that of the ideal-tiling vertices; however, subsequent crossings at larger  $|\mathbf{g}^\perp|$  are noticeably different. This indicates that the perp-space profile of the atomic surface is *not* exactly given by (19).

### 3.3 Integration over diffuse wings

Some of the intensity lost to diffuse scattering is recovered when one integrates over the diffuse wings around each Bragg peak; *some* such integration is always performed due to the resolution function. We did another simulation to test whether this, in some way, undoes the DW reduction.

We summed up the total intensity in a sphere centered on each Bragg point. The sphere radius was 3 grid spacings of the lattice of allowed wavevectors, so it contains 123 wavevectors. (The spacing of our grid of discrete  $\mathbf{q}$  points is reciprocal to the cubic lattice constant 18.87 of the 8/5 approximant, i.e.  $|\Delta\mathbf{q}| = 0.333$  in units of inverse rhombohedron edge. As is visible in Fig. 4, the separation between noticeable Bragg peaks is 6 or 10 grid spacings, i.e.  $\tau^{-1}\pi$  or  $\pi$ , so these spheres do not overlap.) Due to computer time limitations, we only performed this computation for 27 Bragg vectors, selected to be representative of the range of  $g^\perp$  values – a very small fraction of all the usable Bragg vectors.

Fig. 5 also shows these integrated results (crosses). Unexpectedly, the integration seems to restore the same fraction  $c$  of the lost intensity of every peak *independent* of  $g^\perp$  – the same when  $|\mathbf{g}^\perp|$  is so small that the loss is invisible on the figure, and out to peaks where the ideal intensity is down by  $\sim 10^{-2}$  and the random Bragg intensity is down a further  $\sim 10^{-2}$  from the ideal. (Obviously, though,  $c$  depends on the radius of our integration sphere.) The formula for this is

$$I_{I,\text{rand}} = cI_{B,\text{ideal}} + (1 - c)I_{B,\text{rand}} + D, \quad (23)$$

where  $I_{B,\text{ideal}}$  and  $I_{B,\text{rand}}$  are the Bragg intensities for the ideal and random tilings, respectively, and  $I_{I,\text{rand}}$  is the integrated intensity for the random tiling. To get a good fit, we had to include the constant  $D$  which represents some diffuse intensity spread uniformly over reciprocal space.<sup>8</sup> Formula

<sup>7</sup> The positions are a simplification of Ref. [24], but the assignment of species is different. Negative form factors are realized by neutron diffraction for some isotopes. We chose these form factors to make this diffraction pattern as different as possible from that of just the tile vertices.

<sup>8</sup> Uniform diffuse intensity implies, of course, a component of the density that is completely uncorrelated from point to point. We know

<sup>6</sup> If the system size were changed, then of course the Bragg amplitude and the diffuse intensity both scale linearly with the system’s volume.

(23) is plotted for comparison in Fig. 5; Fig. 7 confirms more directly its remarkable success (which is somewhat worse in the decorated model).

It is intriguing to speculate how a fit using the integrated intensities would behave if (23) were exactly correct for real experimental data, particularly if (due, say, to extinction problems) the strong peaks at small  $G_\perp$  were omitted from the fit. Then  $I_{B,\text{rand}}$  could be neglected in (23) and  $I_{I,\text{rand}} \propto I_{B,\text{ideal}}$ , i.e., the ideal structure would be reconstructed (apart from a wrong factor of  $c$  in the absolute normalization of the density).

Note that, inserting the phason Debye-Waller hypothesis of (17) and (18) into (23) implies

$$I_{I,\text{rand}}/I_{B,\text{ideal}} \approx c + (1 - c) (\exp -\sigma^2 |\mathbf{g}^\perp|^2) \quad (24)$$

Thus the *integrated* intensities are *not* expected to be fitted by the phason Debye-Waller form  $I_{I,\text{rand}}/I_{B,\text{ideal}} \approx \exp(-\sigma_I^2 |\mathbf{g}^\perp|^2)$ . However, if the  $|\mathbf{g}^\perp|$  values are so small that  $\exp(-\sigma^2 |\mathbf{g}^\perp|^2) \approx 1 - \sigma^2 |\mathbf{g}^\perp|^2$ , the fit will give an apparent  $\sigma_I^2 \approx (1 - c)\sigma^2$ . Indeed, a smaller value  $\sigma^2$  was fitted by de Boissieu for low-resolution data than for high-resolution data in Ref. [28].

### 3.3.1 Overall transfer to diffuse intensity

A key issue in Sec. 2 was what fraction of intensity is transferred to diffuse scattering in a random tiling. We investigated this using the same random rhombohedral tiling. We summed the total diffuse intensity and the total intensity for all wavevectors lying in the 2-fold plane. The fraction of the total intensity that was “diffuse” was 0.145 in the 3/2 approximant and 0.095 in the 8/5 approximant: the 3/2 approximant shows a strong finite-size effect. This fraction is artificially low in the 2-fold plane which contains many reciprocal lattice vectors with small  $\mathbf{g}^\perp$ . The fraction of *all* intensity which was diffuse was 0.388 in the 3/2 approximant; it was too much to compute in the 8/5 approximant, so we can merely guess it is  $\sim 0.25$  (based on the trend in the 2-fold plane).

### 3.3.2 Digression on diffuse wings

A great deal more can be learned if one measures the detailed shape of the diffuse wings at high resolution, instead of just integrating over them. Diffuse scattering, unlike Bragg scattering, depends on the spatial correlations of disorder.

Elastic theory governs the long-wavelength fluctuations of  $\mathbf{h}^\perp(\mathbf{r})$  in random-tiling-like quasicrystals; energy-stabilized models seem *not* to predict a gradient-squared elasticity [25]. Also, the shape of the diffuse wings of Bragg peaks is a key prediction of the elastic theory [26, 29, 30]. Thus, the match between experiment and elastic theory in *i*-AlPdMn and in *i*-AlCuFe, [31] is evidence that these quasicrystals have a random-tiling nature. (Some of us recently commented on these experiments and calculated some elastic constants, in [22] and [32].)

However, such analysis of diffuse scattering is outside the scope of this paper, which is crystallographic investigations based purely on *Bragg* intensities of many peaks, aimed at discovering the microscopic atomic arrangements.

### 3.3.3 Global diffuse scattering?

An unresolved question, and of relevance to background subtraction, is the diffuse background far away from Bragg peaks. It has been suggested by Ref. [27] that one can account for all of this by summing over the diffuse wings of *all* Bragg peaks, as approximated by elastic theory [26, 29]), even from those that are farther away in reciprocal space than the typical separation of strong Bragg peaks. This is surprising since the elastic theory is a long-wavelength, coarse-grained theory that ought to break down at the corresponding real-space distances (of the order of a tile edge).

In any case, this formula cannot be integrated over all of reciprocal space, since even a single diffuse wing has the schematic form  $\int d^3\mathbf{q} (1/K|\mathbf{q}|^2)$ . It is of interest to write

$$\langle |\mathbf{h}^\perp|^2 \rangle = (2\pi)^{-3} \int_0^{Q_{\text{max}}} d^3\mathbf{q} \frac{3\tilde{e}(K_2/K_1)}{K_1|\mathbf{q}|^2} \quad (25)$$

where the 3 comes from taking the trace of a  $3 \times 3$  matrix, and  $\tilde{e}(K_2/K_1)$  is a dimensionless factor which averages out the angular dependences. For  $K_2/K_1 \ll 1$ , it can be shown that  $\tilde{e} = 1 + (8/9)(K_2/K_1)^2 + \dots$ , while it diverges for  $K_2/K_1 \rightarrow 3/4$  (the usual modulation instability [26]). Noting that  $(K_1, K_2) = (0.8, 0.5)$  for the rhombohedron tiling [20, 21] and  $\tilde{e} \approx 2$ , we obtain  $Q_{\text{max}} \approx 3.5$  which is comparable to  $\pi$  (the spacing between rather strong Bragg peaks).

## 4 Review of tile decoration models

Before going on to the “unified” approach, we will need some more terms and concepts – associated with tilings and their decorations (in real space) – to be used in the two sections following. To start off, we imagine that an ensemble of certain “low-energy” atomic configurations adequately represents the states of the quasicrystal at temperatures below 1000K. Then we insist that every “low-energy” configuration must correspond to a unique tiling. (Hence we sometimes say “tiling” as a shorthand for “atomic configuration represented by the tiling,” *e.g.*, when we speak of “the tiling’s energy.”)

### 4.1 Decoration

The mapping from the tiling to an atomic configuration is called a *decoration*, since each tile of a given class has atoms placed in the same sites on the tile. If necessary, this placement is allowed to have *context dependence* on the neighboring tiles. But if the site is *sometimes* free to receive either of two species, depending on neighboring tiles, it may be preferable to consider this tile as having two “flavors” each with a unique decoration. Sometimes atoms are assigned as decorations of other “tile-objects” such as vertices, edges, or faces, in order to reduce the number of site classes and

no specific defect that does this in our random tiling; the alternation between the two ways of packing four rhombohedra into a rhombic dodecahedron might approximate this.



numerical parameters (see Sec. II A of Ref. [33]). In all this, the principle is that all the constraints and correlations are ascribed to the tiling level, so that the statistics of the tilings contain implicitly all the statistics of the atom configurations.<sup>9</sup>

In random tilings, a rearrangement which turns one valid tile configuration to another, while affecting only a small cluster of tiles, is called a *tile flip*. For a good decoration rule, such that all tilings in the ensemble have similar energies, there is a substantial agreement between the atomic configurations on those tiles before and after the tile flip. (If this weren't so, one of the two configurations would have a much higher energy due to interactions with atoms in neighboring unflipped tiles.) Often, only a couple of atoms change positions in a tile flip.

## 4.2 Supertiles

The close overlap between the “before-flip” and “after-flip” atom configurations often gives us freedom to change the size of tile while only slightly changing the structure model. When switching from large tiles to smaller tiles, the price of using small tiles is some simplifications in the decoration rule, and/or additional constraints among the tiles; the price of using large tiles is having many sites on the tiles with independent parameters. Replacing tiles by supertiles always entails a rebinding [33] of their decorations.

The supertiling phenomenon is particularly prominent in decagons and is already familiar experimentally – particularly in the various subphases of  $d(\text{AlNiCo})$  [34] – and is also known as a cause of mis-indexing [35]. The “inflated” tiles in Penrose’s tiling are a special case of supertile, but most supertiles are not literal inflations. Physically, starting from small tiles with a tile Hamiltonian, the small energy differences between tilings favor a sub-ensemble of degenerate lowest-energy configurations and often these may be represented as tilings with bigger “supertiles”, each decorated in a single way with the original tiles; a special case is the interactions which favor a local pattern or “cluster” [36]. Further remarks on supertilings are in Ref. [37].

## 4.3 Recipe to discover basic structure

To proceed, one must first decide which tiling geometry best represents the structure and its degrees of freedom. Table 4.3 lists a menu of available random tilings which have been used in decoration models of real materials. (Some of the decorations were designed for a quasiperiodic tiling, but are compatible with the random one.) For the tilings marked “no” in column 3 of the table *any* simulation is just barely practical, since each update move must involve an *indefinite* number of tiles. [22, 23, 50].

<sup>9</sup> Decoration models have been formulated such that decorations of different tiles sometimes produce two atoms in the same position, the rule being that these get replaced by one atom. We do not consider such decorations, because in analyzing or optimizing sums over the structure, giving either diffraction amplitudes or total energies, it is awkward when one cannot assign each atom to a well-defined tile-object that it decorates.

**Table 1.** Important tilings for realistic structure models. Under “Local?”, a “yes” means a *local update* exists; only such tilings are easy to simulate. (We have sometimes called the hexagon-boat-star tiling “Two-level”, or the rhombohedral tiling “3DPT”; the latter may also contain rhombic dodecahedra.) Under “symmetry”, ico, 10, and 12 are short for icosahedral, decagonal, and dodecagonal, respectively. References are indicated for tilings and decorations.

Tiling	Symm.	Local?	decorations
rhombohedral [20, 21]	ico	yes	$i(\text{AlPdMn})$ : [38]
canonical cells [39, 40, 41]	ico	no	$i(\text{AlMn})$ : [33, 42]
binary [43, 44]	10	yes	$d(\text{AlCuCo})$ : [45]
hexagon-boat-star [46]	10	yes	$d(\text{AlMn})$ : [47] $d(\text{AlPdMn})$ : [47] $d(\text{AlCuCo})$ : [48] $d(\text{AlNiCo})$ : [49]
rectangle-triangle [50]	10	no	$d(\text{AlPdMn})$ : [50] $d(\text{AlNiCo})$ : [51]
square-triangle [23, 52]	12	no	$dd(\text{VNiSi})$ [53] $dd(\text{Ta}_{1.6}\text{Te})$ [54]

The proper size of the tiles is not self-evident even if, say, one already knows the exact structure of a large approximant crystal. Consider the most extreme case, a structure that looks just like the Penrose tiling. That structure may be broken into tiles at any level of inflation; furthermore, at each level, the tiles may be represented as Fat/Skinny rhombi, as Kites/Darts, as Hexagons/Boats/Stars, or in a couple of other ways. At which level can we break apart the tiles and put them together differently, to build other approximants or random tilings? Only a computation (or intuition) of the energies can tell us.

In the rest of this section, we outline a recipe to find the right tiling, and a coarse version of the structure model, *before* using any diffraction data, from simulations of lattice gases [49], or of random tilings with small tiles, when microscopic Hamiltonians are available. There are four or five stages.

### 4.3.1 Total energy code

Before starting, one must have a means to compute a total energy for any plausible configuration of the atoms forming the quasicrystal. Normally, the best choice is an effective pair potential fitted to, or derived from, ab-initio data [55]. In principle one can use ab-initio energies directly [56], but these are limited to very small system sizes.

### 4.3.2 Lattice gas simulation

Construct a list of (available) sites, forming a quasilattice. The quasilattice constant should be smaller than the inter-atomic spacing, so that the occupied fraction of sites is fairly small compared to unity. A Monte Carlo simulation is carried out (using the Hamiltonian described in Stage 1), in which atoms are allowed to hop as a lattice-gas among these discrete sites; (usually) the temperature is gradually reduced to zero and the final configuration is examined by eye. [57]. This annealing must be repeated over and over, since the system will end up in different final configurations. (That is natural when there are many nearly degenerate states, separated by barriers.)

Although the states are not constrained to be tile decorations, it may turn out that the low-energy states can be represented as such. Discovering this representation is an art,

and there may be more than one correct answer (in that different tiling/decoration combinations might generate identical atomic structures.) The set of possible local patterns found in the resulting tilings implicitly defines a packing or matching rule for the tilings. Thus, the lattice gas simulation serves as a systematic procedure to discover *both* the “right” tiling (with its rules) and the “right” decoration (relating the tiling to atomic positions).

A hybrid random tiling-lattice gas simulation significantly improves on the plain lattice-gas simulation. The system has two kinds of degrees of freedom (both discrete). The first kind is a random tiling (which does *not* need to be the same as the random tiling we are trying to discover by this technique.) Each tile is decorated in a deterministic way by candidate sites: these sites take the place of the quasilattice defined in the plain lattice-gas technique. The second kind of degree of freedom is a lattice gas on these sites. The Monte Carlo simulation must allow tile flips as well as atom hops.

A different kind of hybrid simulation is to use a random tiling of rather small tiles, with a deterministic decoration by atoms. In effect, this is similar to a lattice-gas simulation, in that (with around one atom per tile), practically every topological arrangement of atoms is represented by some tiling.

#### 4.3.3 Simulations of decorated random tilings

At this stage, the degrees of freedom are tiles, and each tiling is decorated deterministically with atoms. A Monte Carlo annealing is performed in which all tilings are allowed, but are weighted as usual by the interaction energy of their atoms. Different variations of the decoration rule are tried out, in an attempt to find the rule which gives final states with the lowest energy. This stage, like stage 2, refines *discrete* degrees of freedom. Also like stage 2, it finds both a decoration rule and tile packing rules, but in a less tentative fashion.

Having carried out stage 3 in small approximant crystals, one then repeats it in larger approximant crystals. (Data from the small approximants could be misleading as there are many local patterns of tiles which can fit in a large approximant or an infinite tiling, but not in a small approximant.)

#### 4.3.4 Optimization of continuous parameters

In this final stage, the decoration is fixed, but decoration parameters such as the atomic coordinates on the tiles are adjusted so as to minimize the total energy. One should still decorate more than one of the final annealed tilings from stage 3.

After stage 4, the decoration and its parameters are finally fixed; the only degree of freedom is tile configurations.

#### 4.3.5 Construction of tile Hamiltonian

The energy can be calculated for each possible tile configuration by decorating it with atoms and using the interatomic pair potentials, but this is time-consuming for a large-size approximant. It may be possible to find, and use, a “tile-Hamiltonian” which is an explicit (and simple) function of the tiles or pairs of neighboring tiles, which accurately mimics the pair-potential energy [33, 42]. This stage could be skipped.

## 5 Unified fit from simulations

The “unified” approach is the second of the two paths for structure determination described in this article. It may be applied after one has a rough or moderately detailed picture of the atomic structure and of the tile degrees of freedom (from related approximants, for example). As noted in the first path, the procedure for fitting the averaged density, after the phase problem is solved, involves fits very similar to those required by the “unified” method, and thus does not deserve a separate discussion.

### 5.1 Random tiling simulation

An honest approach to a random tiling – more precise than the “factorization” approximation of Sec. 3 – requires a simulation, which can be used in several different modes. Mode (i) would be to assume *a priori* a particular random tiling ensemble (that means a fixed list of configurations sampled from a simulation); only the decoration parameters are varied. Mode (ii) would be to hold the decoration parameters fixed and vary the “tile Hamiltonian” parameters to control tile correlations, until an optimum fit is achieved. In this case, every iteration requires a fully equilibrated Monte Carlo simulation of the random tiling; the approximant cell size may be limited by time constraints since we must do repeated Monte Carlo simulations. Mode (iii) would be a “simulated annealing” of the tiling: one performs a Monte Carlo simulation in which the *R*-factor itself replaces the tile Hamiltonian in the Boltzmann factor. As the temperature is reduced, only the tile configurations which optimize the *R*-factor will be represented.

#### 5.1.1 Structure determination assisted by energy calculations

We strongly believe in the need to combine diffraction and energy inputs to structure determination, because they contain complementary information.<sup>10</sup> For example, some rare atoms are impossible to pin down by diffraction, but very easy to decide on the basis of energies. Again, transition-metal atoms from the same row ordinarily cannot be distinguished by X-ray diffraction, but they can be clearly assigned by the use of potentials[49].

In fact, exactly the same strategies can be applied either to the energy values or to the diffraction data. For example, one could run through all the steps of the “Recipe” in Subsec. 4.3 minimizing, instead of the total energy, the *R*-factor for the fit to a diffraction data set. (In a diffraction fit, the parameters appearing in the Stage 3 description might include Debye-Waller factors or partial occupations.) While it is desirable to run energy and diffraction fits separately, the “most realistic” fit should do them in parallel, minimizing some linear combination of the total energy and the *R*-factor (or the  $\chi^2$ ) quantifying the mismatch to the measured Bragg intensities. (This would be similar in spirit to the method of “least-squares with energy minimization” in ordinary crystallography [58].

<sup>10</sup> The familiar invocation of “steric constraints” to rule out unphysically close atoms could be considered an informal application of energy information.

## 5.2 Technical issues in simulations for diffraction fitting

Here we discuss how one might, in practice, do an iterative calculation which combines (i) Monte Carlo reshuffling of the random tiling; (ii) computation of Fourier sums to obtain the structure factors; and (iii) adjustment of parameters to optimize the fit.

### 5.2.1 Simulation cell as an approximant

A simulation, of course, can only be done in a finite system, normally with periodic boundary conditions. Periodicity forces a net background phason strain; this is minimized when the simulation cell has the size and shape of the unit cell of a good rational approximant of the quasiperiodic tiling. To calculate the diffraction, we repeat this cell's configuration throughout space. Hence reciprocal space has a very fine grid of Bragg peaks, but most of them have negligible intensity even for an approximant of an ideal quasiperiodic tiling. Of the Bragg peaks identifiable in the ideal case, most are lost in the random-tiling case. (Their intensity is greatly reduced by what is loosely called the perp-space Debye-Waller factor, while meanwhile a uniform diffuse background appears almost everywhere in reciprocal space; the Bragg intensity is overwhelmed if it is several times smaller than the diffuse intensity.)

Each orbit of equivalent quasicrystal Bragg peaks breaks up into several orbits of inequivalent Bragg peaks of the approximant. We should average their amplitudes, to reduce the systematic error (due to phason strain) and the statistical error (from the finite size or time of the random-tiling simulation). Before doing such an averaging, one must be careful to shift the unit cell so that the different approximant amplitudes have the same phase. If the approximant is big enough, the inequivalent amplitudes should be nearly the same.

The deviations from symmetry always grow with the perp-space reciprocal lattice vector  $\mathbf{g}^\perp$ . Meanwhile, the intensities decrease with  $\mathbf{g}^\perp$ . So the simulation cell should preferably be big enough so that, with increasing  $\mathbf{g}^\perp$ , the intensities become unmeasurable (or lost in the diffuse scattering) before the deviations from icosahedral symmetry become overwhelming. But often the simulation cell must be small, for the technical reasons we turn to next.

### 5.2.2 Structure factor sum

In all cases, one must re-evaluate structure factors repeatedly – in the case of mode (iii), at every *step* of the iteration. Even if the cell has relatively few tiles, it still has more atoms than any unit cell of a metal crystal. (For example, for the canonical cell tiling, the smallest reasonable approximant is the  $3/2$  cubic cell, which contains typically 32 tile nodes (112 tiles), but some 2500 atoms.) Summing the exponentials is relatively expensive in computer time, and the Fast Fourier Transform appears to be useless since the sites do not lie on a simple grid. Thus, the simulation cell size may be limited by the diffraction sum.

One can save work by partially factorizing the sums. Let the index  $\mu$  label the type of tile (or tile-object), and let the (many) allowed orientations of each tile-object be indexed by  $\omega$ . Let  $n_\mu$  be the number of site type on tile-object

$\mu$ , according to the decoration rule in use, and let  $\nu$  be the index labeling them; also let  $M_{\mu\nu}$  be the multiplicity of sites of type  $\mu\nu$  on tile-object  $\mu$ . Finally, let  $N_{\mu\omega}$  be the number of tile-objects of type  $\mu$  and orientation  $\omega$  in the tiling. Then we can define the “tile structure factors” as

$$F_{\mu\omega}^{\text{tile}}(\mathbf{q}) = \sum_{j=1}^{N_{\mu\omega}} \exp[i\mathbf{q} \cdot \mathbf{R}_{\mu\omega j}] \quad (26)$$

where  $\mathbf{R}_{\mu\omega j}$  is the reference point of the  $j$ -th tile-object of type  $\mu$  in orientation  $\omega$ .

Also, we can define the “decoration structure factors” as

$$F_{\mu\nu\omega}^{\text{deco}} = \sum_{i=1}^{M_{\mu\nu}} f_{a(\mu\nu)}(\mathbf{q}) \exp[i\mathbf{q} \cdot \mathbf{u}_{\mu\omega\nu i}] \quad (27)$$

Here  $\mathbf{u}_{\mu\omega i}$  is the displacement of the decorating atom from the reference point of that tile-object,  $a(\mu\nu)$  is the atom species in orbit  $\mu\nu$ , and  $f_a(\mathbf{q})$  is the form factor for species  $a$ . Note that  $F_{\mu\nu\omega}^{\text{deco}}$  for different orientations  $\omega$  is trivially obtained from some reference orientation simply by applying the corresponding rotation or reflection to  $\mathbf{q}$ . This symmetry can reduce the labor, though, only if that rotation or reflection takes one of the allowed  $\mathbf{q}$  vectors to another one.

The total structure factor then takes the form

$$F(\mathbf{q}) = \sum_{\mu\omega} F_{\mu\omega}^{\text{tile}}(\mathbf{q}) F_{\mu\nu\omega}^{\text{deco}}(\mathbf{q}). \quad (28)$$

In a mode (i) process, the first factor remains fixed in every term; in mode (ii), the second factor remains fixed. Furthermore, it is easy to compute the *change* in  $\{F_{\mu\omega}^{\text{tile}}\}$  due to each Monte Carlo update move, and this usually affects relatively few of the different  $\mu\omega$  types. Similarly, if we change a parameter in the decoration rule, we only need to update  $F_{\mu\nu\omega}^{\text{deco}}$  for the orbit  $\mu\nu$  which that parameter applies to.

## 6 Decagonals

Decagonal materials present special problems.<sup>11</sup> The greatest problem is the seductiveness of *apparent* two-dimensionality, which makes it so much easier to visualize the tile packings than in icosahedral cases. In fact, however, the stacking is crucial. *Physically*, it must amplify interactions within the layers and thus make the structure more ordered than a two-dimensional model could be (and perhaps more ordered than analogous icosahedral models are). In *imaging* of the structure, averaging may produce highly symmetrical patterns even when these are not really present in individual layers.

### 6.1 Stacking randomness

First of all, the equilibrium random tiling phase of a decagonal *cannot* be modeled by a random two-dimensional

<sup>11</sup> The same considerations would apply to the other stacked quasicrystals (octagonal and dodecagonal).

tiling [1, 59]. The entropy, which is supposed to stabilize such a phase, would be proportional to the two-dimensional extent of the system and (in the thermodynamic limit) would be negligible compared to the volume. (A corollary of this is that simulations of decagons with simulation cells just one lattice constant thick in the  $c$  direction do not give a valid picture of the tiling randomness. However they *are* valid for discovering which atom arrangements are energetically favored, and which tiling is appropriate to model that composition.)

Instead, one must permit stacking randomness<sup>12</sup> that is, the tiling configuration is similar but not identical from one layer to the next. The difference between adjacent layers is constrained by rules exactly analogous to the packing rules that determine how tiles may adjoin within a layer. Unfortunately, stacking randomness seems to be the least understood aspect of decagonal structures, both experimentally [60, 61] and theoretically. [62] Like everything else in decagons, the stacking rules might depend sensitively on composition.

## 6.2 Images

We repeat an old warning about high-resolution transmission electron microscope (HRTEM) images. When a sample is thick enough that a typical vertical section crosses a stacking change, then the image becomes (roughly speaking, and ignoring the dynamical effects) a two-dimensional projection of the scattering density. That projection is always perfectly quasiperiodic, and can not reveal the randomness of individual layers.[1, 21].

For this reason, we implore the practitioners of HRTEM (and other techniques that project along the direction of the electron beam, such as the high-angle annular dark-field method discussed elsewhere in this volume): please try to determine the thickness of the crystal! The perfection of the image can be evidence for the perfection of the quasicrystal only to the extent that an upper bound is placed on the thickness.

Multi-layer simulations of a realistic model of  $i(\text{AlNiCo})$  are feasible [49] but not yet realized. We propose that a superposition of time steps, as shown in Fig. 8, is a good ersatz for a superposition of layers. The reason is that the 2D tilings in adjacent layers should differ by elementary tile flips in isolated places, and the same thing is true for configurations of time-evolving 2D tilings separated by small steps. (The main qualitative difference is that the superposition of layers is *less* random, at long wavelengths, than that of time steps, as discussed in Sec. 6.6 of Ref. [1].)

The point that Fig. 8 is intended to illustrate is that clusters of (near) 10-fold symmetry emerge from the projection which are *not* present in any layer. Furthermore, to accomplish this, one does not need drastic differences

from one layer to the next. This is intended to be a caution about structure models derived from electron microscopy, by assuming that the image can be interpreted as a two-dimensional structure (made of two layers). Even more so, it is a caution that the symmetrical ring motifs, which are so striking visually in the images, do not necessarily correspond to an atomic motif.

## 6.3 Supertilings

A final caution about interpreting HRTEM patterns will be obvious to most of the microscopists, but perhaps not to others. *Supertiles* (see Sec. 4) are much commoner in decagonal than in icosahedral phases.<sup>13</sup> Quite typically – in analyzing experimental images or simulated configurations [49, 63] – the structure is manifestly a packing of certain small tiles (or clusters). Yet they are highly constrained, so one suspects that a description in terms of a supertiling would be more economical. But which one is correct? From initial data, perhaps, one can conjecture that certain configurations are forbidden, and we can show this implies that the allowed configurations are exactly decorations of a certain simple supertiling. Yet we then notice (in larger simulation cells) one or two exceptions, indicating that the real rule is more complicated. (Although wrong, the simple supertiling is not useless – it might be quite adequate for a fit of the available diffraction data.)

This observation is intended as a second caution about reducing HRTEM images to tilings by placing nodes at the centers of pentagonal or decagonal rings of spots. In the actual images, there is often a continuum of patterns between (say) symmetrical rings and distorted rings: one must almost arbitrarily include some nodes and exclude others. Small differences in this rule, or errors in its application, may induce major changes in the rules of the inferred tiling, in the sense that a previously forbidden local pattern may start to appear, or vice versa.

## 7 Conclusion

All steps of the procedure for fitting a random-tiling structure are now available in principle, but they have not yet been put into practice. Even though a new kind of “direct method” may determine the phases of Bragg amplitudes (Sec. 2); this merely produces the ensemble-averaged scattering density; there remains the harder task of modeling the random-tiling ensemble which has been averaged. In accomplishing this, it seems hard to disentangle energy modeling from structure modeling. Indeed we suspect that the best structure fits of the future will combine total energy calculations and diffraction refinements in some fashion.

In principle, a simple perp-space Debye-Waller factor should *not* suffice to model the relation between the ideal and random tilings, but in practice this seemed to work

<sup>12</sup> We used the term “randomness” rather than “disorder”, which would connote deviation from a particular, ideal structure. In the random tiling case, the ideal structure is inherently random. The stacking randomness is that a layer disagrees with the adjacent layers, not with an ideal layer. We do *not* have in mind stacking disorder of the Hendricks-Teller kind, e.g. adjacent layers of type A when the normal pattern alternates type A and type B layers.

<sup>13</sup> One reason may be that the natural inflation scale for a decagonal is only  $\tau = (\sqrt{5} + 1)/2$  compared to  $\tau^3$  for a simple icosahedron, which as mentioned in Sec. 3.1.1, is often appropriate in models of face-centered icosahedral structures.

rather well for the rhombohedron tiling (Sec. 3). More study is needed: it would be interesting, for example, to apply the “minimum-charge” method of Sec. 2 to the Monte Carlo “data” of Sec. 3. And if one is given only the random-tiling data, what sort of ideal tiling will be reconstructed from it if we adopt the factorization approximation and divide out the best-fit Debye-Waller factors?

Decagonal structures are deceptive. They are easy to visualize using two-dimensional images, but the equilibrium random ensemble is *never* represented by a two-dimensional tiling. It should be a priority – both in experiment and in total-energy modeling – to understand the stacking randomness in decagonals.

At the very start of this paper, we demanded a model which contains information beyond the averaged density: implicitly that means information about correlations. Yet we set “rules of the game” which restricted us to using only Bragg data, discarding the diffuse intensity which is in fact the Fourier transform of the correlation function. So, an interesting question for the future is whether there is some systematic way to incorporate *diffuse* data from all of reciprocal space (not merely wings of Bragg peaks) in a quantitative fit of parameters of a random tiling structure model.

**Acknowledgments.** We thank K. Brown and A. Avanesov for help in the phase computations and for producing figures 1 and 2. We thank them, as well as R. Hennig, M. de Boissieu, E. Cockayne, M. Widom, and M. E. J. Newman, for discussions, comments, and collaborations. C.L.H. and M.M. were supported by DOE grant No. DE-FG02-89ER-45405. Computer facilities were provided by the Cornell Center for Materials Research under NSF grant DMR-9632275. V. E. was supported by NSF grant 9873214.

## References

- [1] Henley, C. L.: Random tiling models. Steinhardt, P. J., DiVincenzo, D. P. (Eds.): *Quasicrystals: The State of the Art*, p. 429. World Scientific, 1991.
- [2] Janot, C.: *Quasicrystals: a primer*. Oxford University Press, 1994
- [3] Elser, V.: Indexing problems in quasicrystal diffraction. *Phys. Rev. B* 32 (1985) 4892-4898.
- [4] Elser, V.: The diffraction pattern of projected structures. *Acta Crystallogr. A* 42 (1986) 36; Duneau, M., and Katz, A.: Quasiperiodic patterns. *Phys. Rev. Lett.* 54 (1985) 2688-2691.
- [5] Widom, M.: Entropically stabilized quasicrystals. Jarić, M. V. and Lundqvist, S. (Eds.): *Quasicrystals*, p. 337 (World Scientific, 1989); Henley, C. L., Random tilings and real quasicrystals. Yacamán, M. Y., Romeu, D., Castaño, V., Gómez, A. (Eds.): *Quasicrystals and Incommensurate Structures in Condensed Matter*, p. 152. (World Scientific, 1990).
- [6] Stephens, P. W.: The icosahedral glass model. Jarić, M. V., Gratias, D. (Eds.): *Aperiodic Crystals III: Extended Icosahedral Structures*, p. 37 (Academic Press, 1989).
- [7] Socolar, J. E. S.: Locality constraints and 2D Quasicrystals. Jarić, M. V., Lundqvist, S.: *Quasicrystals*, p. 182 (World Scientific, Singapore, 1990).
- [8] de Boissieu, M., Janot, C., Dubois, J.-M.: Quasi-crystal structure: cold water on the Penrose tiling scheme. *J. Phys. Condens. Matter* 2 (1990) 2499-2517.
- [9] Cornier-Quiquandon, M., Quivy, A., Lefebvre, S., Elkaim, E., Heger, G., Katz, A., Gratias, D.: Neutron-diffraction study of icosahedral Al-Cu-Fe single quasicrystals. *Phys. Rev. B* 44 (1991) 2071-2084. Cornier-Quiquandon, M., Gratias, D., Katz, A.: A tentative methodology for structure determination in quasicrystals. Pérez-Mato, J. M., Zúñiga, F. J., Madariaga, G. (Eds.): *Methods of structural analysis of modulated structures and quasicrystals* pp. 313-332. (World Scientific, Singapore, 1991).
- [10] Qiu, S.-Y., Jarić, M. V.: Quasicrystal structure determination: Al-Cu-Li. Jarić, M. V., Lundqvist, S. (Eds): *Quasicrystals*, p. 19 (World Scientific, Singapore, 1990).
- [11] Elser, V.: X-ray phase determination by the principle of minimum charge. *Acta Crystallogr. A* 55 (1999) 489.
- [12] Elser, V., in preparation.
- [13] Nemhauser, G. L., Wolsey, L. A. *Integer and Combinatorial Optimization* (Wiley Interscience, 1988).
- [14] Harker, D., Kasper, J. S.: Phases of Fourier coefficients directly from crystal diffraction data. *Acta Crystallogr. A* 1 (1948) 70.
- [15] Avanesov, A., Brown, K., Elser, V., in preparation.
- [16] Boudard, M., deBoissieu, M., Janot, C., Heger, G., Beeli, C., Nissen, H.-U., Vincent, H., Ibberson, R., Audier, M., Dubois, J.-M.: Neutron and X-ray single-crystal study of the AlPdMn icosahedral phase. *J. Phys. Condens. Matter* 4 (1992) 10149-10168.
- [17] DeBoissieu, M., Janot, C., Dubois, J.-M.: Diffraction studies of quasi-crystals: the truncation effects in six-dimensions. *Europhys. Lett.* 7 (1988) 593-598.
- [18] de Boissieu, M., Stephens, P., Boudard, M., Janot, C., Chapman, D. L., Audier, M.: Anomalous X-ray diffraction study of the AlPdMn icosahedral phase *J. Phys. Condens. Matter* 6 (1994) 10725-10745.
- [19] Boudard, M., Letoublon, A., de Boissieu, M., Ishimasa, T., Mori, M., Elkaim, E., Lauriat, J. P.: Phase Transition and Diffuse Scattering studies in the AlCuFe ternary system. *Proceedings of ICQ7* (1999), to appear.
- [20] Tang, L.-H.: Random-Tiling Quasicrystal in Three Dimensions. *Phys. Rev. Lett.* 64 (1990) 2390-2393.
- [21] Shaw, L. J., Elser, V., Henley, C. L.: Long-range order in a three-dimensional random tiling quasicrystal. *Phys. Rev. B* 43 (1991) 3423-3433.
- [22] Mihalković, M., Henley, C. L., unpublished.
- [23] Oxborrow, M., Henley, C. L.: Random square-triangle tilings: A model for twelvefold-symmetric quasicrystals. *Phys. Rev. B* 48 (1993) 6966-6998.
- [24] Henley, C. L., Elser, V.: Quasicrystal structure of (Al, Zn)<sub>49</sub>Mg<sub>32</sub>. *Philos. Mag. Lett.* B 53 (1986) L59-66.
- [25] Lubensky, T. C., Ramaswamy, S., Toner, J.: Hydrodynamics of icosahedral quasicrystals. *Phys. Rev. B* 32 (1985) 7444-7452. Lubensky, T. C.: Symmetry, elasticity, and hydrodynamics in quasiperiodic structures. M. V. Jarić (Ed.): *Aperiodic Crystals I: Introduction to Quasicrystals*, p. 199 (Academic Press, London, 1988), and references therein.
- [26] Widom, M.: Elastic stability and diffuse scattering in icosahedral quasicrystals. *Philos. Mag. Lett.* 64 (1991) 297-305. Ishii, Y.: Phason softening and structural transitions in icosahedral quasicrystals. *Phys. Rev. B* 45 (1991) 5228-5239.
- [27] Capitan, M. J., Calvayrac, Y., Quivy, A., Joulaud, J. L., LeFebvre, S., Gratias, D.: X-ray diffuse scattering from icosahedral Al-Pd-Mn quasicrystals. *Phys. Rev. B* 60 (1999) 6398-6404.
- [28] de Boissieu, M., Stephens, P., Boudard, M., Janot, C., Chapman, D. L., Audier, M.: Disorder and complexity in the atomic structure of the perfect icosahedral alloy Al-Pd-Mn. *Phys. Rev. Lett.* 72 (1994) 3538-41; see Fig. 3 in particular.
- [29] Jarić, M. V., Nelson, D. R.: Diffuse scattering from quasicrystals. *Phys. Rev. B* 37 (1988) 4458-4472.
- [30] Mori, M., Ishimasa, T., Kashiwase, Y.: X-ray diffuse scattering of an Al-Cu-Fe single quasicrystal. *Philos. Mag. Lett.* 64 (1991) 49-57.
- [31] de Boissieu, M., Boudard, M., Hennion, B., Bellissent, R., Kycia, S., Goldman, A., Janot, C., Audier, M.: Diffuse scattering and phason elasticity in the AlPdMn icosahedral phase. *Phys. Rev. Lett.* 75 (1995) 89-92; Boudard, M., de Boissieu, M., Letoublon, A., Hennion, B., Bellissent, R., Janot, C.: Phason softening in the AlPdMn icosahedral phase. *Europhys. Lett.* 33 (1996) 199-204.
- [32] Zhu, W.-J., Henley, C. L.: Phonon-phason coupling in icosahedral Quasicrystals. *Europhys. Lett.* 46 (1999) 748-754.
- [33] Mihalković, M., Zhu, W.-J., Henley, C. L., Oxborrow, M.: Al-Mn Decoration Models: I. Geometrical Principles. *Phys. Rev. B* 53 (1996) 9002-9020.
- [34] Ritsch, S., Beeli, C., Nissen, H.-U., Gödecke, T., Scheffer, M., Lück, R.: The existence regions of structural modifications in decagonal AlCoNi. *Philos. Mag. Lett.* 78 (1998) 67-76.

- [35] Lançon, F., Billard, L., Burkov, S., de Boissieu, M.: On choosing a proper basis for determining structures of quasicrystals. *J. Physique France I* **4** (1994) 283-301.
- [36] Jeong, H.-C., Steinhardt, P. J.: Cluster Approach for Quasicrystals. *Phys. Rev. Lett.* **73** (1994) 1943-1946; Jeong, H.-C., Steinhardt, P. J.: Constructing Penrose-like tilings from a single prototile and the implications for quasicrystals. *Phys. Rev. B* **55** (1997) 3520-3532. See also Henley, C. L.: Cluster maximization, non-locality, and random tilings. Takeuchi, S., Fujiwara, T. (Eds): *Quasicrystals*, p. 27 (World Scientific, 1998).
- [37] Roth, J., Henley, C. L., Frank-Kasper decagonal quasicrystals: simulations and ideal models. *Philos. Mag.* **A75** (1997) 861-887.
- [38] Elser, V.: Random tiling structure of icosahedral quasicrystals. *Philos. Mag. B* **73** (1996) 641-656.
- [39] Henley, C. L.: Cell geometry for cluster-based quasicrystal models. *Phys. Rev. B* **43** (1991) 993-1020.
- [40] Mihalkovič, M., Mrafkó, P.: Tiling of canonical cells: large Pa3 approximants. *Europhys. Lett.* **21** (1993) 463-467.
- [41] Newman, M. E. J., Henley, C. L., Oxborrow, M.: Construction of periodic approximants for the canonical-cell model of a quasicrystal. *Philos. Mag. B* **71** (1995) 991-1013.
- [42] Mihalkovič, M., Zhu, W.-J., Henley, C. L., Phillips, R.: Al-Mn Decoration Models: II. Optimization under Realistic Potentials. *Phys. Rev. B* **53** (1996) 9021-9045.
- [43] Widom, M., Strandburg, K. J., Swendsen, R. H.: Quasicrystal equilibrium state. *Phys. Rev. Lett.* **58** (1987) 706-709; Lançon, F., Billard, L., Chaudhari, P.: Thermodynamical properties of a two-dimensional quasicrystal from molecular dynamics calculations. *Europhys. Lett.* **2** (1986) 625-629.
- [44] Strandburg, K. J.: Random-tiling quasicrystal. *Phys. Rev. B* **40** (1989) 6071-6084.
- [45] Burkov, S. E.: Structure Model of the Al-Cu-Co Decagonal Quasicrystal. *Phys. Rev. Lett.* **67** (1991) 614-617.
- [46] Tang, L.-H., Jarič, M. V.: Equilibrium quasicrystal phase of a Penrose tiling model. *Phys. Rev. B* **41** (1990) 4524-4546.
- [47] Li, X. Z., Kuo, K. H.: A new Al-Mn approximant and the structure of the Al-Mn decagonal quasicrystal. Kuo, K. H., Ninomiya, T. (Eds.): *Proc. of Chinese-Japan Seminars on Quasicrystals*, pp. 103-110 (World Scientific, 1991).
- [48] Cockayne, E., Widom, M.: Ternary Model of an Al-C-Co Decagonal Quasicrystal. *Phys. Rev. Lett.* **81** (1998) 598-601.
- [49] Mihalkovič, M., Al-Lehyani, I., Widom, M., Henley, C. L., Moriarty, J., Wang, Y., Magudam, N., in preparation.
- [50] Oxborrow, M., Mihalkovič, M. Random-tiling disorder and the diffuse scattering of the decagonal AlPdMn quasicrystal. de Boissieu, M., Verger-Gaugry, J.-L., Currat, R. (Eds): *Aperiodic '97*, p. 451 (World Scientific, 1998). Note that  $d(\text{AlPdMn})$  actually corresponds to a "constrained" variant of the rectangle-triangle tiling, as explained in the reference.
- [51] Mihalkovič, M., unpublished.
- [52] Widom, M.: Bethe Ansatz Solution of the Square-Triangle Random Tiling Model. *Phys. Rev. Lett.* **70** (1993) 2094-2097. Kalugin, P. A.: The square-triangle random-tiling model in the thermodynamic limit. *J. Phys. A* **27** (1994) 3599-3614. Kalugin, P. A.: Low-lying excitations in the square-triangle random tiling model. *J. Phys. A* **30** (1997) 7077-7087.
- [53] Chen, H., Li, D. X., Kuo, K. H., New type of two-dimensional quasicrystal with twelvefold rotational symmetry. *Phys. Rev. Lett.* **60** (1988) 1645-1648.
- [54] Krumeich, F., Conrad, M., Harbrecht, B.: *Proc. 13th Intl. Conference on Electron Microscopy (ICEM 13) vol. 2*, p. 752 (1994); Conrad, M., Harbrecht, B.: Structural properties of  $\text{Ta}_{97}\text{Te}_{60}$  and  $\text{Ta}_{181}\text{Te}_{112}$ , two approximants of a dodecagonal tantalum telluride. de Boissieu, M., Verger-Gaugry, J.-L., Currat, R. (Eds): *Aperiodic '97*, p. 205 (World Scientific, 1998).
- [55] Hafner, J., *The Structures of Binary Compounds*, (Elsevier, 1989); Windisch, M., Hafner, J., Krajčí, M., Mihalkovič, M.: Structure and lattice dynamics of rational approximants to icosahedral Al-Cu-Li. *Phys. Rev. B* **49** (1994) 8701-8717; Zou, J., Carlsson, A. E.: Preferred Mn Spacing in Al-Mn Compounds. *Phys. Rev. Lett.* **70** (1993) 3748-3751; Moriarty, J. A., Widom, M.: First-principles interatomic potentials for transition-metal aluminides: theory and trends across the 3d series. *Phys. Rev. B* **56** (1997) 7905-7917.
- [56] Hennig, R. G., Majzoub, E. H., Carlsson, A. E., Kelton, K. F., Henley, C. L., Yelon, W. B., Kresse, G., Hafner, J.: Constructing approximants for the TiZrNi quasicrystals. *Proc. ICQ7*, to appear.
- [57] Cockayne, E., Widom, M.: Structure and phason energetics of Al-Co decagonal phases. *Philos. Mag.* **A77** (1998) 593-619.
- [58] Jack, A., Levitt, M.: Refinement of large structures by simultaneous minimization of energy and R factor. *Acta Crystallogr. A* **34** (1978) 931-935.
- [59] Burkov, S.: Are layered two-dimensional quasicrystals periodic in the third direction? *J. Stat. Phys.* **65** (1991) 395-401.
- [60] Ritsch, S., Nissen, H.-U., Beeli, C.: Phason related stacking disorder in decagonal Al-Co-Ni. *Phys. Rev. Lett.* **76** (1996) 2507-10.
- [61] Wittmann, R.: Comparing different approaches to model the atomic structure of a ternary decagonal quasicrystal. *Z. Kristallogr.* **214** (1999) 501-505.
- [62] Shin, M., Strandburg, K. J.: Random tiling approach to the structure of decagonal quasicrystals. *J. Non-Cryst. Solids* **153-154** (1993) 253-257.
- [63] Cockayne, E., personal communication (1999).



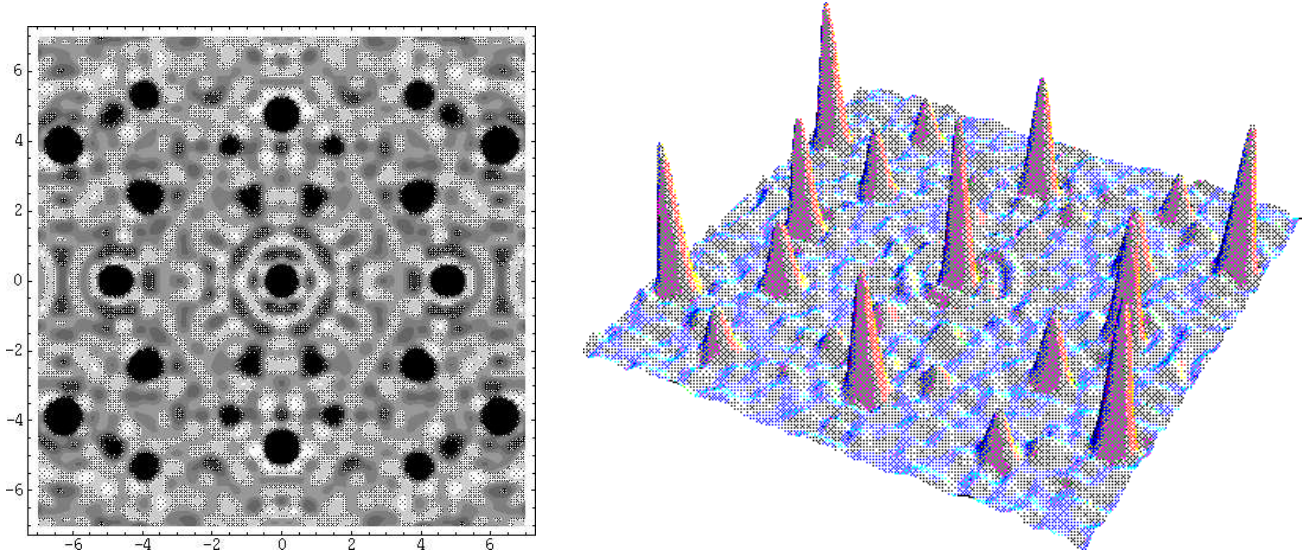


**Fig. 1.** Average electron density  $\rho(\mathbf{r})$  of  $i(\text{AlPdMn})$  in physical space, reconstructed from 503 experimental x-ray structure factors of [16] using signs obtained by the minimum charge algorithm of Sec. 2. The plane of the plot is an icosahedral mirror plane ( $13\text{\AA} \times 13\text{\AA}$ ) centered on a pseudo-Mackay cluster ( $n_0$  atomic surface). Charge density is represented by darkness in (a) and by height in (b). There are several instances of atoms (or partial atoms) at unphysically short separation.

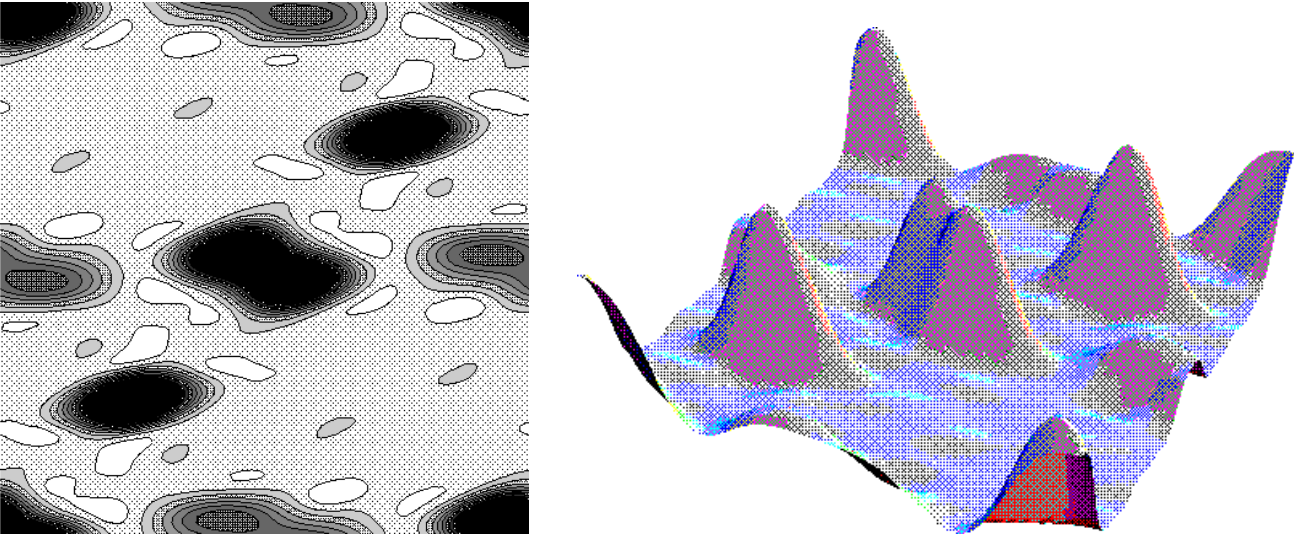


**Fig. 2.** The same electron density plotted in Figure 1 but for the 5-fold periodic plane. The figure box is a unit cells of this plane, so the physical and perp space directions run obliquely. The  $n_0$  surface is centered at  $(0, 0)$  and  $(1/2, 1/2)$ ,  $n_1$  at  $(1/2, 0)$  and  $(0, 1/2)$ , and  $bc_1$  at  $(1/4, 1/4)$  and  $(3/4, 3/4)$ . A  $\tau^3$  inflation has been applied to both plots to make the rounding of features in parallel and perp-space comparable in magnitude (i.e. so the respective Debye-Waller factors are similar); this is seen most clearly in the contour plot (a). The height plot (b) shows that the density profile of the  $n_0$  “surface” even in the perp-direction, is rounded to an extent comparable to its entire width.

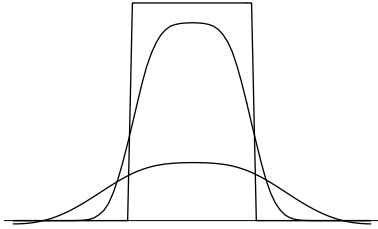


**Fig. 3.** Cross section  $\rho(\mathbf{h}^\perp)$  of atomic surface, for ideal and random rhombohedron tilings. The horizontal axis is a one-dimensional section along the twofold direction; the vertical scale is normalized so the integral of the density  $\int d^3\mathbf{h}^\perp \rho(\mathbf{h}^\perp)$ , approximated as spherically symmetric, is the same. The rectangular and the flat-topped curves are the ideal and random rhombohedron tilings, respectively. The very broad Gaussian is a scan through the  $bc_1$  atomic surface reconstructed from Boudard's data [16] using the minimum-charge method of Sec. 2. (The horizontal scale is converted to units of rhombohedron edges assuming the model of Ref. [38].) This last curve differs from a section of Fig. 2 in that only 300 reflections are used here.



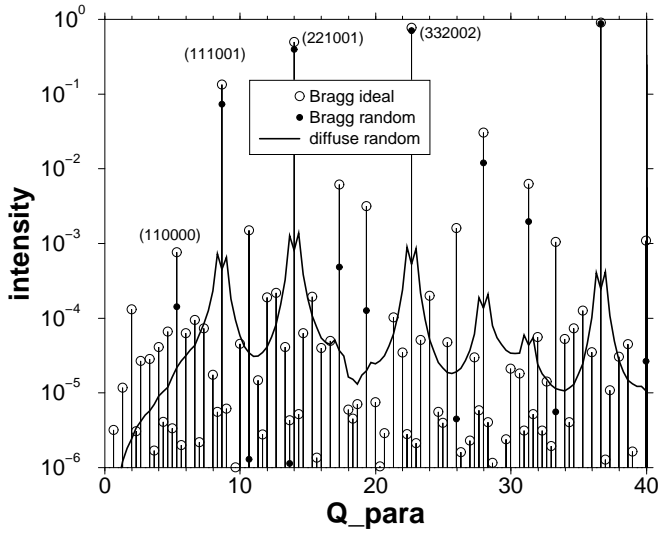


**Fig. 4.** Separate Bragg and diffuse diffraction along the 2-fold axis of reciprocal space for the rhombohedron random tiling (8/5 approximant). Vertical bars are a guide for the eye and indicate the location of the Bragg peaks. All reciprocal lattice vectors are included with intensity over  $10^{-6}$ . Some peaks are labelled using Elser's convention [3]. The same figure was presented by Tang in Ref. [20], but without separating the Bragg and diffuse parts.

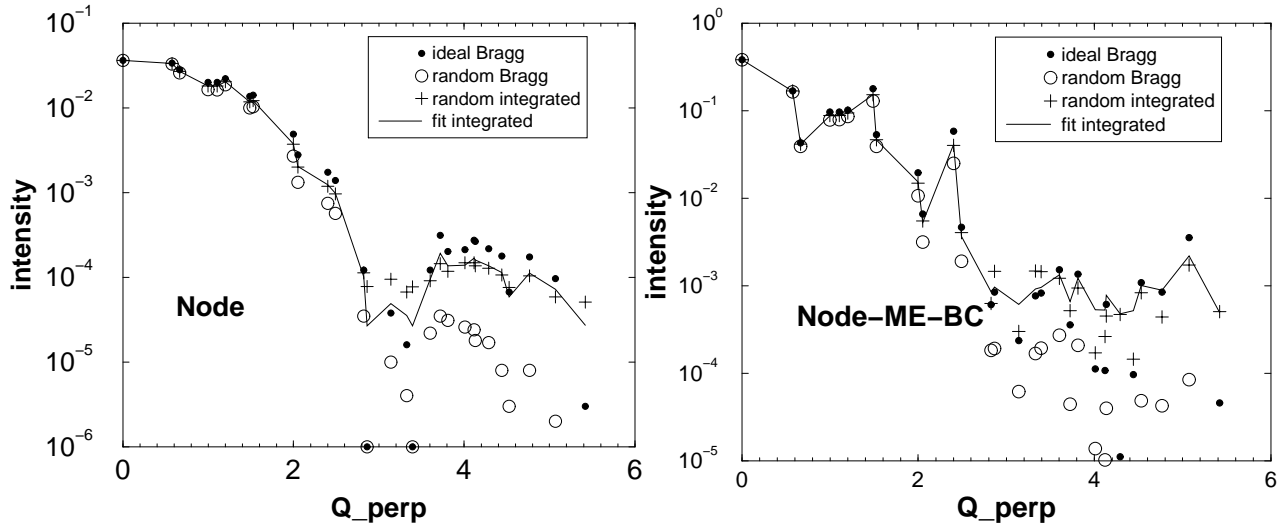


**Fig. 5.** Diffraction intensities from simulated ideal and random tilings, as a function of perp wavevector. Filled circles: Bragg peak intensities  $I_{B,\text{ideal}}$  from ideal 3D Penrose tiling (3DPT) of rhombohedra. Empty circles: Bragg intensities  $I_{B,\text{rand}}$  from the random 3DPT. Crosses: total intensities  $I_{I,\text{rand}}$  from the random 3DPT, integrated over a sphere centered on the Bragg peak, to be compared with the solid line representing eq. 23; see Sec. 3.3. Plot (a) shows diffraction from the tiling nodes only, fitted by  $c = 0.51$ ,  $D = 3.0 \times 10^{-5}$ . Plot (b) is from a decoration in which node points have form factor +1, while the midedge and “body-center” points (on axis of each prolate rhombohedron) have form factor -1; this is fitted by  $c = 0.47$  and  $D = 4.7 \times 10^{-4}$  in eq. (23). Note: in this and the next two figures,  $|\mathbf{g}^\perp|$  is called “Q-perp” on the figure axis label.)

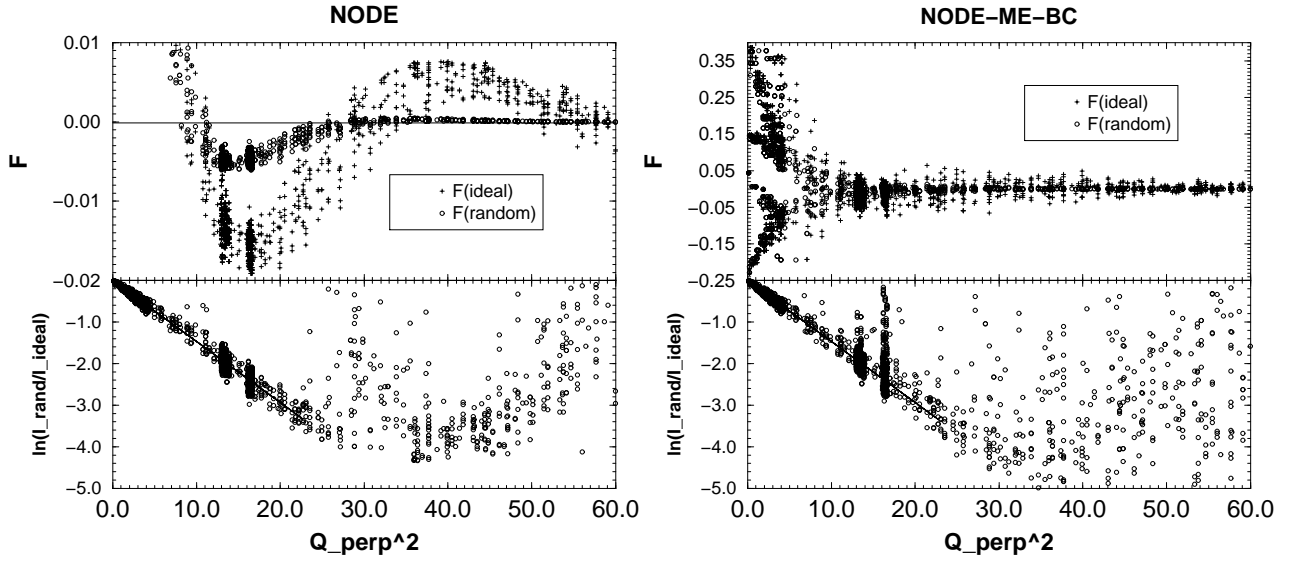


**Fig. 6.** Perp Debye-Waller factor in random tiling. At top  $|F(\mathbf{g}^\perp)|$  is plotted for the ideal and the random tiling, showing the intensity reduction. At bottom, the effective DW factor,  $2W_{\text{eff}}$  from eq. (22), is plotted against  $|\mathbf{g}^\perp|^2$  (labeled “Q\_perp^2” in the figure); its dependence is linear out to the second node of  $F(\mathbf{g}^\perp)$ , showing the validity of the simple formula (18) out to surprisingly large wavevectors. Plot (a) shows diffraction from the tiling nodes only; plot (b) is from a decoration in which node points have form factor +1, while the midedge and “body-center” points (on the axis of each prolate rhombohedron) have form factor  $-1$ .

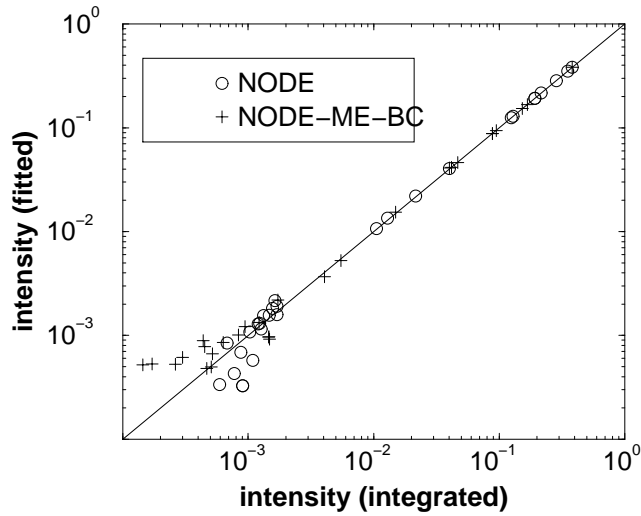


**Fig. 7.** The same data as in Fig. 5(a) are plotted here (circles) as a comparison of the integrated intensity with the fit from eq. (23), using the coefficients  $c$  and  $D$  mentioned in the caption of Fig. 5(a). The crosses represent a similar comparison for the decorated model shown in Figs. 5(b) and 6(b).

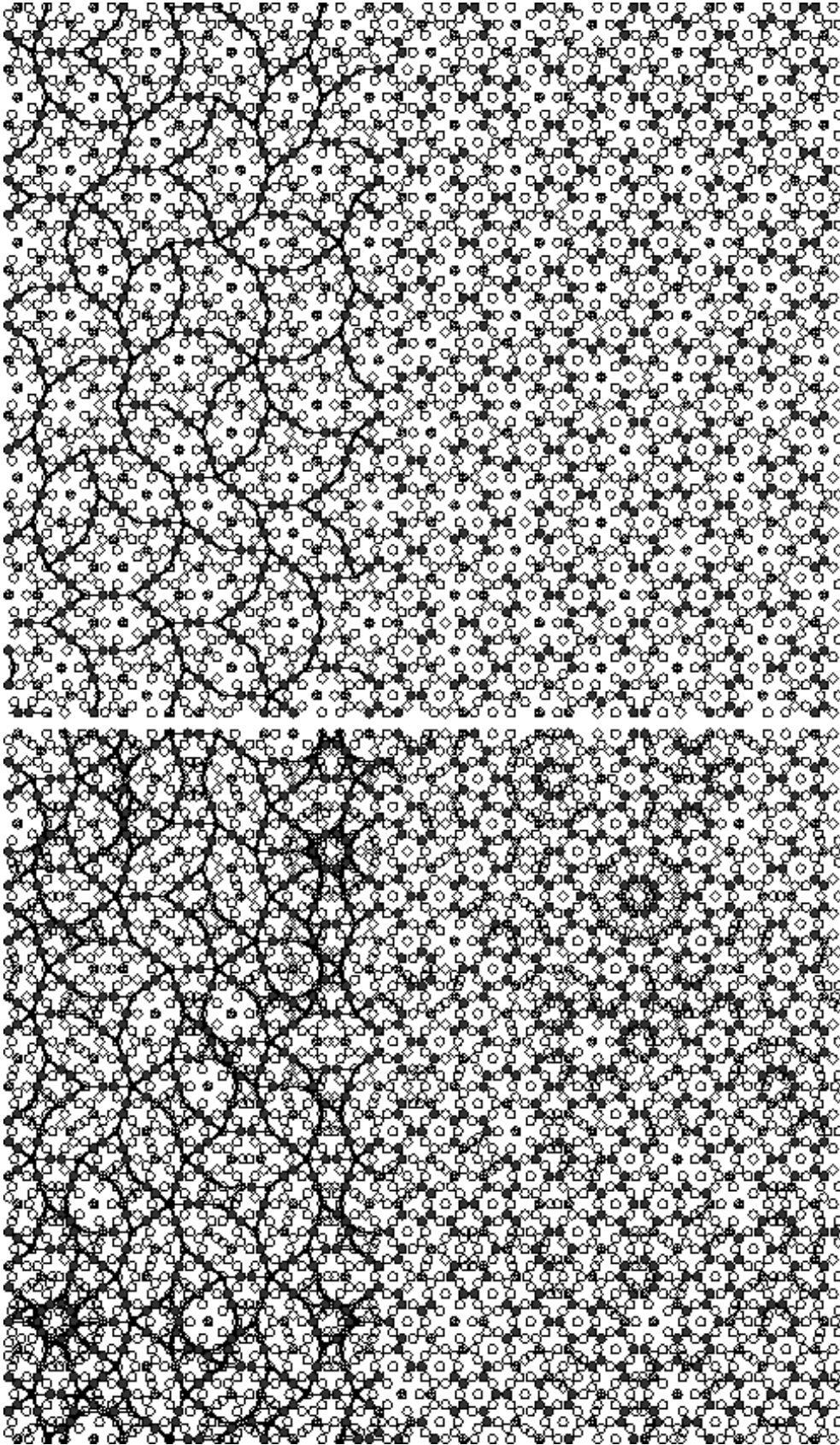


**Fig. 8.** Top, a snapshot from one time step in a simulation of the (maximally) random Hexagon-Boat-Star tiling. The tiling is decorated with atoms (Ni and Co shown filled), as in the  $d(\text{AlNiCo})$  model of Ref. [49]. The tile edges are drawn in only in the left portion. Bottom, a superposition of nine successive time steps; see how clusters of tenfold symmetry emerge that are not present in the snapshot. This is a poor man's imitation of a superposition of different layers, as viewed in an HRTEM image.